Development 140, 82-92 (2013) doi:10.1242/dev.082172

A Hh-driven gene network controls specification, pattern and size of the *Drosophila* simple eyes

Daniel Aguilar-Hidalgo[1,2,*], María A. Domínguez-Cejudo[1,*], Gabriele Amore[3], Anette Brockmann[1,‡], María C. Lemos[2], Antonio Córdoba[2] and Fernando Casares[1,§]

SUMMARY

During development, extracellular signaling molecules interact with intracellular gene networks to control the specification, pattern and size of organs. One such signaling molecule is Hedgehog (Hh). Hh is known to act as a morphogen, instructing different fates depending on the distance to its source. However, how Hh, when signaling across a cell field, impacts organ-specific transcriptional networks is still poorly understood. Here, we investigate this issue during the development of the *Drosophila* ocellar complex. The development of this sensory structure, which is composed of three simple eyes (or ocelli) located at the vertices of a triangular patch of cuticle on the dorsal head, depends on Hh signaling and on the definition of three domains: two areas of *eya* and *so* expression – the prospective anterior and posterior ocelli – and the intervening interocellar domain. Our results highlight the role of the homeodomain transcription factor *engrailed* (*en*) both as a target and as a transcriptional repressor of *hh* signaling in the prospective interocellar region. Furthermore, we identify a requirement for the *Notch* pathway in the establishment of *en* maintenance in a Hh-independent manner. Therefore, *hh* signals transiently during the specification of the interocellar domain, with *en* being required here for *hh* signaling attenuation. Computational analysis further suggests that this network design confers robustness to signaling noise and constrains phenotypic variation. In summary, using genetics and modeling we have expanded the ocellar gene network to explain how the interaction between the Hh gradient and this gene network results in the generation of stable mutually exclusive gene expression domains. In addition, we discuss some general implications our model may have in some Hh-driven gene networks.

KEY WORDS: Ocellus, *hedgehog*, Patterning, Mathematical model, Retinal determination genes, Gene network, *Drosophila*, *engrailed*, *Notch*

INTRODUCTION

During development, gradients of intercellular signals (called morphogens) are read and modified dynamically by fields of target cells. As a result, spatiotemporal patterns of gene expression are generated. These patterns are then translated into cell function and into the development of functional body structures (Freeman and Gurdon, 2002; Davidson, 2006). Yet how the integration between intercellular signals and intracellular gene networks occurs is only beginning to be understood.

One of the best characterized family of morphogens is that of *hedgehog* (*hh*). Hh genes are evolutionarily conserved and participate in many key developmental processes. Not surprisingly, their malfunction has been associated with a number of developmental diseases and with cancer (Jiang and Hui, 2008; Varjosalo and Taipale, 2008; Ingham et al., 2011). Experimental work in *Drosophila* and in vertebrates indicates that the Hh signaling pathway is subject to extensive feedback among elements of the pathway, most notably that of the Hh receptor *patched* (*ptc*) (Chen and Struhl, 1996; Marigo and Tabin, 1996). Furthermore, the combination of experimental and modeling studies on developing fly wings and on vertebrate neural tube and limbs have uncovered new roles for this feedback in the dynamics of Hh gradient formation, in its robustness and in the generation of distinct patterns of target gene expression (Briscoe et al., 2001; Saha and Schaffer, 2006; Dessaud et al., 2007; Dessaud et al., 2008; González et al., 2008; Nahmad and Stathopoulos, 2009; Dessaud et al., 2010; Irons et al., 2010; Probst et al., 2011; Balaskas et al., 2012). Therefore, the iteration between mathematical modeling and experimentation is emerging as a productive way of illuminating the problem of Hh morphogen action during organ growth and patterning. Here, we investigate this issue in a particularly simple and genetically tractable model organ: the *Drosophila* ocellar complex.

The *Drosophila* ocelli are three simple eyes [one anterior (or medial) ocellus and two posterior (or lateral) ocelli] located at the vertices of a triangular patch of cuticle on the dorsal head. Together, the ocelli and the interocellar cuticle (plus its bristles) are referred to as the 'ocellar complex' (Fig. 1A). The development of the ocellar complex depends on *hh*. Flies homozygous for a *hh* temperature-sensitive mutation raised at the restricted temperature during larval development (Royet and Finkelstein, 1996) or expressing a dominant-negative Ptc receptor [PtcΔloop2 (Briscoe et al., 2001)] lack the ocellar complex (Fig. 1B). Therefore, *hh* signaling is required for the specification and pattern of two tissue types: ocellus and interocellar cuticle.

The ocellar complex forms by the fusion of the dorsal-anterior domains of the eye discs (Haynie and Bryant, 1986). Here, the ocellar field is specified by the action of, at least, two transcription factors: the pax6 gene *twin of eyeless* (*toy*) and the Otx family member *orthodenticle* (*otd*) (*ocelliless*, *oc* – FlyBase) (Finkelstein et al., 1990; Wieschaus et al., 1992; Royet and Finkelstein, 1995; Punzo et al., 2002; Blanco et al., 2010; Wang et al., 2010; Brockmann et al., 2011). *hh* is expressed within the ocellar field in the prospective interocellar region (Royet and Finkelstein, 1996;

[1]CABD (CSIC-UPO-Junta de Andalucía), Sevilla 41013, Spain. [2]Condensed Matter Physics Department Universidad de Sevilla, Sevilla 41012, Spain. [3]Istituto Regionale Vini e Oli di Sicilia, Palermo 90143, Italy.

*These authors contributed equally to this work
‡Present address: University of Konstanz, Konstanz 78457, Germany
§Author for correspondence (fcasfer@upo.es)

Accepted 21 September 2012

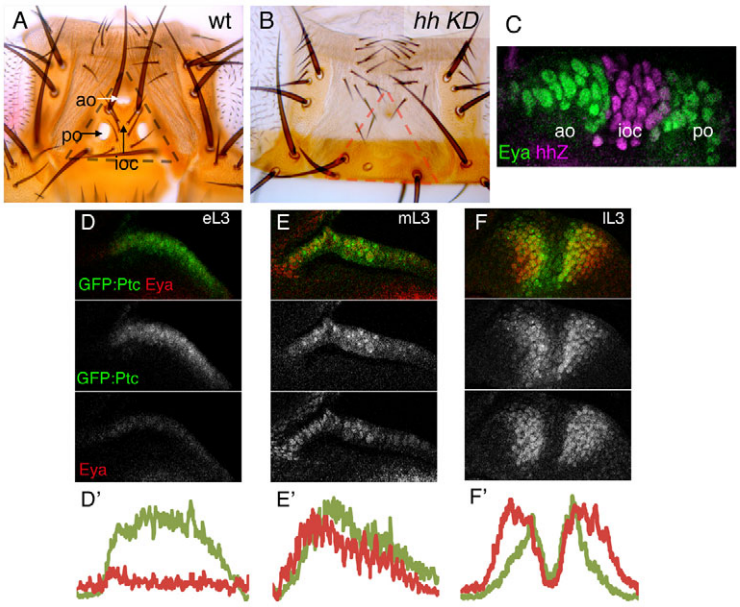

Fig. 1. Dynamic *hh* signaling and the development of the ocellar complex. (**A**,**B**) Dorsal views of adult heads from wild-type (A) or *oc2>ptcΔloop2* (*hh* signaling knock down; *hhKD*). The ocellar complex is outlined by the triangle. Anterior ocellus (ao), posterior ocellus (po) and interocellar cuticle (ioc) are marked. All elements of the ocellar complex are obliterated when the *hh* signaling pathway is blocked. (**C**) Ocellar region of a late L3 disc from a *hhZ* larvae. The β-galactosidase-expressing domain (magenta; *hhZ*) labels the prospective interocellar cuticle (ioc) and is flanked by two domains of Eya expression (green) in the prospective anterior (ao) and posterior (po) ocelli. This orientation (anterior towards the left) will be maintained throughout. (**D-F'**) Prospective ocellar regions of early ('e', D), mid ('m', E) and late ('l', F) third instar (L3) GFP:Ptc larvae, stained for anti-Eya. GFP signal was detected directly. Merged and single channels are shown. Below, signal intensity histograms of both GFP:Ptc (green) and Eya (red) signals of the respective discs. GFP:Ptc, which is used as a read-out of the Hh signaling, is initially expressed at high an uniform levels through the region (D-E'), to later evolve into a high-low-high pattern (F,F'). Eya expression is detected at low and uniform levels in eL3 (D,D'), to then increase as a single domain in mL3 (E,E'), which is later transformed into a high-low-high pattern similar to Ptc (F,F').

Royet and Finkelstein, 1997). The retinal determination (RD) genes *eyes absent* (*eya*) and *sine oculis* (*so*) are required for the formation of the ocelli (Bonini et al., 1993; Cheyette et al., 1994; Serikaku and O'Tousa, 1994; Bonini et al., 1998; Blanco et al., 2009; Blanco et al., 2010; Brockmann et al., 2011). Both *eya* and *so* are expressed with identical patterns in two domains flanking *hh*, and mark the prospective ocelli in late third larval (L3) stage discs (Blanco et al., 2009). The expression of *eya* and *so* depends on secreted Hh and on their mutual positive feedback (Pauli et al., 2005; Blanco et al., 2009). In addition to the activation of *eya* and *so,* expression of the TALE-homeodomain transcription factor *homothorax* (*hth*) is concomitantly repressed in the ocellar domains. Otherwise, maintenance of *hth* expression prevents ocellar development (Brockmann et al., 2011).

In this paper, we have investigated how the single domain of *hh* expression is capable of generating the ocellar pattern through the regulation of a downstream gene network using both genetic and modeling approaches.

MATERIALS AND METHODS

Drosophila strains and genetic manipulations

oc2-GAL4 (Blanco et al., 2009) was used to drive UAS lines specifically in the developing dorsal anterior region of the eye-antennal imaginal disc (EAD), where the ocellar region derives from. In the case of UASdsRNAi strains, crosses were raised at 29°C, to maximize the penetrance of the knock-downs. Other crosses were set at 25°C. UAS lines used were as follows: UAS-GFP-*ptc*Δloop2 [UAS-ptcDN (Briscoe et al., 2001)], UAS-*ci* (Alexandre et al., 1996), UAS-*mamDN* (dominant negative) (Kumar and Moses, 2001) and UAS-*en* (Guillén et al., 1995; Tabata et al., 1995); the *hedgehog* transcriptional reporter line hh^{P30} (referred to herein as *hh-Z*) and the *engrailed* transcriptional reporter line en^{Xho25} (referred to herein as *en-Z*), which are from the Bloomington Stock Center (http://flystocks.bio.indiana.edu); and UAS-*Dl*RNAi (28032) and UAS-*Su(H)*RNAi (103597), which are from the VDRC (http://stockcenter.vdrc.at/control/main). The GFP:Ptc strain [CB02030 from Flytrap (http://flytrap.med.yale.edu/) (Buszczak et al., 2007)] is a GFP-protein trap that tags the Ptc product. Two reference strains, Oregon-R (Or-R) and w^{1118}, and stocks carrying mutant alleles for *patched* [*ptc: yw; FRT42 ptc*^{S2}*/CyO* (BL # 6332)], *smoothened* (*smo: w; smo*^{3} *FRT40A/CyO*), *cubitus interruptus* (*ci: ywhsflp; Ci+ FDT40A /CyO ;; Ci*^{94}) and *Notch* [*N: w[ch2], N*$^{264\text{-}39}$*/FM4, B[+]* (BL # 730)] are described in FlyBase.

The flip-out method (Basler and Struhl, 1994) was used to induce gain-of-function clones. Clones were induced 48-72 hours after egg laying (AEL) by a 10 heat-shock at 35.5°C in larvae from the cross of *yw, hs-flp, act>hsCD2>Gal4;UAS-lacZ* females with UAS-*hth*GFP males (*hth+* clones) or *yw, hs-flp, act>hsCD2>Gal4;UAS-GFP* females with UAS-*en* males (*en+* clones). *en* loss-of-function clones were generated through mitotic recombination (Xu and Rubin, 1993) in *yw, hs-flp; FRT42D Df(2R)en*^{E}*/FRT42D, ubiGFP* larvae. *Df(2R)enE* deletes both the *engrailed* and *invected* paralogous genes (described in FlyBase). Clones were induced 48-72 hours AEL by a 45 heat-shock at 37°C. Clones were marked in larval tissues by the absence of GFP. Adult heads from this experiment were mounted and their dorsal head examined for ocellar field defects. Clones were not marked in the adult.

Adult cuticle preparation and quantifications

Dorsal head cuticle pieces were dissected from adult or late pharate heads in PBS, and mounted in Hoyers solution:acetic acid (1:1), as described previously (Casares and Mann, 2000). Images were obtained in a Leica DM500B microscope with a Leica DFC490 digital camera and processed with Adobe Photoshop. Ocellar (longest axis) and interocellar lengths were measured with ImageJ (http://imagej.nih.gov/ij/) on digital images and expressed in pixels.

Immunostaining and imaging

Immunofluorescence was carried out as described previously (Bessa and Casares, 2005). Antibodies used were: guinea pig anti-Hth (Casares and Mann, 2000), guinea pig anti-So (Mutsuddi et al., 2005), rabbit anti β-galactosidase (Cappel), mouse anti-Ptc (Nakano et al., 1989), mouse anti-Eya (10H6), mouse anti-En (4D9), mouse anti-Dl (C594.9B) and rat anti-CiA (2A1) [which detects the activator form of Ci (Aza-Blanc et al., 1997; Méthot and Basler, 1999); all from the Developmental Studies Hybridoma Bank, University of Iowa (http://dshb.biology.uiowa.edu)]. Appropriate Alexa-conjugated secondary antibodies were used. Nuclei were counterstained with DAPI. Image acquisition was carried out in an Apotome Zeiss Axio Imager M2 fluorescence microscope and a Leica SME confocal system. Images were processed with Adobe Photoshop.

Expression profiles

Confocal sections of GFP:ptc eye discs at different stages of L3 development, and co-stained with anti-Eya, were selected. To ensure that only signal coming from the prospective ocellar regions were analyzed, each of these regions was outlined with the lasso tool, copied and pasted on a black background and saved as a TIFF file, using Adobe Photoshop. The expression profiles were obtained from these TIFF files using ImageJ.

Temperature fluctuation assay

A temperature fluctuation assay was carried out essentially as previously (Li et al., 2009). Embryos were collected for 24 hours (at 25°C) and grown for an additional 24 hours at 25°C and then transferred to 31°C until larvae reached third instar. Then, larvae were subjected to five cycles of temperature pulses (1.5 hours at 18°C + 1.5 hours at 31°C). After these pulses, cultures were maintained at 25°C until eclosion. As controls, the same strains were grown at constant 25°C throughout development.

Model implementation

A simplified one-cell model (13 equations) was implemented using Vensim software, a visual tool for solving ODEs that allows parameter values modification in run-time (Vensim PLE version 5.11, Ventana Systems, http://www.vensim.com/software.html). This program contains a fourth order Runge Kutta method (RK4) to solve ODE systems. The 31-cell full model was implemented using MATLAB and solved with the integrator ode45.

Complete list of model equations and general descriptions

Each of the 13 differential equations of the reaction-diffusion type describes the behavior of one system variable (gene transcription and protein production) in a row of 31 cells with a symmetrical distribution of cells centered on the morphogen source (five middle cells). Equation 1 describes the classical evolution of a morphogen (Hh) gradient with production and diffusion terms. In this model, the level of complexity was increased by adding a negative regulation, as formation of Ptc/Hh complexes reduces dynamically the concentration of free Hh. The production term is limited to the *hh*-expressing cells, as expressed in Eqn 14.

Following von Dassow et al. (von Dassow et al., 2000), all other equations distinguish between mRNA transcription and translation. Translation is described using linear terms of production and degradation. Transcriptional regulation is described using non-linear terms, either positive or negative, in the form of compound Hill equations. The specific form of these type of terms is $\phi(X\psi(Y,k2,n2),k1,n1)$, where $\phi(X,k,n)=X^n/(k^n+X^n)$ and $\psi(Y,k,n)=1-Y^n/(k^n+Y^n)$. The ocellar model contains autoregulations. In these cases, the equation term is described as a simple sigmoid in the form $\phi(X,k,n)$ (see supplementary material Appendix S1 for further details). For each species, the equation takes specific forms, depending on its specific regulatory relationships (for example, with or without autoregulation term).

The model contains different parameter types: α_x for the basal transcription rates, β_x for the degradation rates, k_x for the Hill equation transcriptional regulators, n_x for the Hill coefficients, θ_x for the translation rates and γ_x for protein complex formation. The non-dimensional parameters k_0, k_{Ci}, k_{En} and k_{Ciptc} are used for changing the scale of different terms and D is the diffusion coefficient. Subscript X-Y, with X and Y system variables, indicates regulation from X to Y. For example, $k_{En\text{-}ptc}$ is the Hill transcriptional regulation parameter of the interaction from En to *ptc*. All the reaction-diffusion equations contain a degradation term.

$$\frac{\partial Hh}{\partial t} = D\frac{\partial^2 Hh}{\partial x^2} + \delta(x)\alpha_{hh} - \gamma_{Ptc-Hh}Ptc\cdot Hh - \beta_{Hh}Hh \quad (1)$$

$$\frac{\partial ptc}{\partial t} = \kappa_0\beta_{ptc}\left\{\left[\alpha_{ptc} + \kappa_{Ciptc}\frac{Ci_A^{n_{Ci_A}}\left(1-\frac{Ci_R^{n_{Ci_R}}}{k_{Ci_R}^{n_{Ci_R}}+Ci_R^{n_{Ci_R}}}\right)^{n_{Ci_A}}}{k_{Ci_A}^{n_{Ci_A}}+Ci_A^{n_{Ci_A}}\left(1-\frac{Ci_R^{n_{Ci_R}}}{k_{Ci_R}^{n_{Ci_R}}+Ci_R^{n_{Ci_R}}}\right)^{n_{Ci_A}}}\right]\cdot\left(1-\frac{En^{n_{En-ptc}}}{k_{En-ptc}^{n_{En-ptc}}+En^{n_{En-ptc}}}\right) - ptc\right\} \quad (2)$$

$$\frac{\partial Ptc}{\partial t} = \theta_{ptc}\,ptc - \gamma_{Ptc-Hh}Ptc\cdot Hh - \beta_{Ptc}Ptc \quad (3)$$

$$\frac{\partial PtcHh}{\partial t} = \gamma_{Ptc-Hh}Ptc\cdot Hh - \beta_{PtcHh}PtcHh \quad (4)$$

$$\frac{\partial ci}{\partial t} = \kappa_0\beta_{ci}\left\{\frac{\alpha_{ci}\left(1-\frac{En^{n_{En-ci}}}{k_{En-ci}^{n_{En-ci}}+En^{n_{En-ci}}}\right)^{n_{Ci}}}{k_{ci}^{n_{ci}}+\left(1-\frac{En^{n_{En-ci}}}{k_{En-ci}^{n_{En-ci}}+En^{n_{En-ci}}}\right)^{n_{Ci}}} - ci\right\} \quad (5)$$

$$\frac{\partial Ci_A}{\partial t} = \kappa_0\beta_{Ci_A}\left(\theta_{ci}ci - Ci_A\right) - \kappa_{Ci}\frac{Ci_A^{n_{Ci_A}}\left(1-\frac{\left(\frac{PtcHh}{Ptc}\right)^{n_{PH}}}{k_{PH}^{n_{PH}}+\left(\frac{PtcHh}{Ptc}\right)^{n_{PH}}}\right)^{n_{Ci_A}}}{k_{Ci_A}^{n_{Ci_A}}+Ci_A^{n_{Ci_A}}\left(1-\frac{\left(\frac{PtcHh}{Ptc}\right)^{n_{PH}}}{k_{PH}^{n_{PH}}+\left(\frac{PtcHh}{Ptc}\right)^{n_{PH}}}\right)^{n_{Ci_A}}} \quad (6)$$

$$\frac{\partial Ci_R}{\partial t} = \kappa_{Ci}\frac{Ci_A^{n_{Ci_A}}\left(1-\frac{\left(\frac{PtcHh}{Ptc}\right)^{n_{PH}}}{k_{PH}^{n_{PH}}+\left(\frac{PtcHh}{Ptc}\right)^{n_{PH}}}\right)^{n_{Ci_A}}}{k_{Ci_A}^{n_{Ci_A}}+Ci_A^{n_{Ci_A}}\left(1-\frac{\left(\frac{PtcHh}{Ptc}\right)^{n_{PH}}}{k_{PH}^{n_{PH}}+\left(\frac{PtcHh}{Ptc}\right)^{n_{PH}}}\right)^{n_{Ci_A}}} - \kappa_0\beta_{Ci_R}Ci_R \quad (7)$$

$$\frac{\partial en}{\partial t} = \kappa_0\beta_{en}\left\{\left[\alpha_{en} + \frac{Ci_A^{n_{Ci_A}}\left(1-\frac{Ci_R^{n_{Ci_R}}}{k_{Ci_R}^{n_{Ci_R}}+Ci_R^{n_{Ci_R}}}\right)^{n_{Ci_A}}}{k_{Ci_A}^{n_{Ci_A}}+Ci_A^{n_{Ci_A}}\left(1-\frac{Ci_R^{n_{Ci_R}}}{k_{Ci_R}^{n_{Ci_R}}+Ci_R^{n_{Ci_R}}}\right)^{n_{Ci_A}}}\right] + \kappa_{En}\frac{En^{n_{En}}}{k_{DlEn}^{n_{En}}+En^{n_{En}}} - en\right\} \quad (8)$$

$$\frac{\partial En}{\partial t} = \theta_{en}en - \beta_{En}En \quad (9)$$

$$\frac{\partial eya}{\partial t} = \kappa_0\beta_{eya}\left\{\alpha_{eya} + \frac{\alpha_{Toy}Ci_A^{n_{Ci_A}}\left(1-\frac{Hth^{n_{Hth}}}{k_{Hth-eya}^{n_{Hth}}+Hth^{n_{Hth}}}\right)^{n_{Ci_A}}}{k_{Ci_Aeya}^{n_{Ci_A}}+Ci_A^{n_{Ci_A}}\left(1-\frac{Hth^{n_{Hth}}}{k_{Hth-eya}^{n_{Hth}}+Hth^{n_{Hth}}}\right)^{n_{Ci_A}}} + \frac{Eya^{n_{Eya}}}{k_{Eya}^{n_{Eya}}+Eya^{n_{Eya}}} - eya\right\} \quad (10)$$

$$\frac{\partial Eya}{\partial t} = \theta_{eya}\, eya - \beta_{Eya}\, Eya \tag{11}$$

$$\frac{\partial hth}{\partial t} = \kappa_0 \beta_{hth} \left\{ \frac{\alpha_{hth} + \alpha_{Wg}\left(1 - \frac{Eya^{n_{Eya}}}{k_{Eya-hth}^{n_{Eya}} + Eya^{n_{Eya}}}\right)^{n_{Wg}}}{k_{Wg}^{n_{Wg}} + \left(1 - \frac{Eya^{n_{Eya}}}{k_{Eya-hth}^{n_{Eya}} + Eya^{n_{Eya}}}\right)^{n_{Wg}}} - hth \right\} \tag{12}$$

$$\frac{\partial Hth}{\partial t} = \theta_{hth}\, hth - \beta_{Hth}\, Hth \tag{13}$$

$$\delta(x) = \begin{cases} 1 \text{ if } x \in hh\text{-expressing cells} \\ 0 \text{ if } x \notin hh\text{-expressing cells} \end{cases} \tag{14}$$

RESULTS

Hh signaling and *eyes absent* expression are dynamic during ocellar patterning

In order to understand how the ocellar pattern (Fig. 1C) was generated, we analyzed the expression of *ptc* (a Hh signaling readout) and *eyes absent* (*eya*) (a Hh target) in the prospective ocellar region throughout L3. To monitor Ptc expression, we used a GFP:Ptc protein trap line. In early L3 discs, we detected a single domain of GFP:Ptc expression and uniformly low levels of Eya (Fig. 1D). By mid-L3, levels of Eya rise within the GFP:Ptc-expressing region, also as a single domain (Fig. 1E). From mid to late-L3, the final pattern arises through the repression of Ptc/Eya expression in the prospective interocellar cuticle (Fig. 1F). This pattern suggests the existence of a repressor capable of attenuating the *hh* pathway in the middle of the ocellar field [see also Brockmann et al. (Brockmann et al., 2011)] and whose expression and/or activity should build up during L3.

engrailed is activated by Hh and attenuates its signaling pathway to establish the ocellar pattern

engrailed (*en*) is a candidate *hh* repressor. It encodes a homeodomain transcription factor with an additional transcriptional repressor domain (Jaynes and O'Farrell, 1991). En is known to repress transcription of two major *hh* signaling components, *ptc* and *ci*, in embryos and wing imaginal discs (Eaton and Kornberg, 1990; Hidalgo and Ingham, 1990; Sanicola et al., 1995; Schwartz et al., 1995; Domínguez et al., 1996; Biehs et al., 2010). In the wing, *hh* expression in its posterior compartment depends on *en*. However, *hh* signaling from the posterior compartment induces *en* expression in anterior cells at a short range. Therefore, *en* is a low sensitivity *hh* target in the anterior wing (Guillén et al., 1995; Ohlmeyer and Kalderon, 1998; Méthot and Basler, 1999). In the ocellar region, *hh* expression precedes that of *en*, which is expressed in a *hh*-like pattern in late L3 (Royet and Finkelstein, 1996). These results suggest that *en* could be a *hh* target in the ocellar region. To test this point, we first checked the relative expression of *hh*, using the *hh-Z* strain as a *hh* transcriptional reporter, and of *en*. Their domains almost completely overlapped, with some En-only cells adjacent to the *hh-Z* domain (Fig. 2A). Second, when we knocked down the *hh* signaling pathway in *oc2>GFP-PtcΔloop2* discs, *en* expression was lost. The expression of *so*, which follows that of *eya*, was also lost from the ocellar region, confirming the effectiveness of the knock-down (Fig. 2B). This result indicated that *en* is a *hh* pathway target

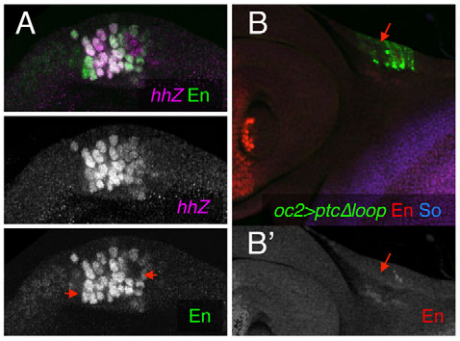

Fig. 2. *en* is a *hh*-signaling target. (A-B′) Ocellar fields of late-L3 larvae. (**A**) *hh-Z* larva stained for β-galactosidase ('hh-Z') and anti-En. Individual channels are shown. The red arrows indicate nuclei expressing En, but not β-galactosidase. (**B**,**B′**) *oc2>ptcΔloop2-GFP* larva, stained for En and So. The expression of *ptcΔloop2* is detected in the ocellar field as the GFP-positive patch (arrows). In this region, the *en* expression is almost totally absent. The En channel is shown separately (B′). In this genotype, So expression is also lost, indicating that the *hh*-signaling knock down induced by overexpression of *ptcΔloop2* is effective.

in the ocellar region. To test for *en* function, we carried out three experiments. First, we verified the status of the *hh* signaling pathway in the *en*-expressing cells by examining *ci* expression. In the *en* domain, *ci* is repressed (Fig. 3A), a fact that is consistent with the repressor role of *en* in other developmental contexts. Second, to test directly this repressing role, we induced marked clones of cells homozygous for the *Df(2R)enE*. This deficiency removes both *en* and its paralog *invected* (*inv*), thus avoiding potential functional redundancy between both genes. In *Df(2R)enE* clones spanning the ocellar field the expression of Ptc and Ci is now continuous, lacking the characteristic gap in the prospective interocellar region (Fig. 3B). In adult mosaics, the anterior and posterior ocelli are often fused (Fig. 3C). The fact that the area of the fused ocelli is larger than the sum of the wild-type anterior and posterior ones suggests that the increase in ocellar surface is at the expense of interocellar cuticle. And third, we checked the effects of *en* overexpression on the *hh* target *eya*. In GFP-marked *en*-expressing clones, *eya* is repressed in a cell-autonomous manner (Fig. 3D). This *eya* loss could be explained either by *en* directly repressing *eya* or, indirectly, by *en* blocking the *hh* pathway. To distinguish between these two possibilities, we overexpressed *ci* throughout the ocellar field in *oc2>ci* larvae, therefore making *ci* transcription insensitive to *en* regulation. In these larvae, the expression of both *eya* and *en* is detected in most of the ocellar field (Fig. 3E,F). Therefore, Ci can activate *eya* even in the presence of *en*. In *oc2>ci* adults, the resulting ocellar complex is composed of a large, single ocellus, without interocellar cuticle (Fig. 3G). This indicates that *eya* is functionally epistatic over *en*, and suggests that the primary role of *en* is as a *hh* pathway regulator. In all, these results indicate that high concentrations of Hh result in high *en* expression, which in turn attenuates *hh* signaling in the middle of the ocellar field. As a consequence, RD expression and ocellar specification can only occur in regions that flank the *en* domain, which becomes the interocellar domain.

Delta:Notch signaling is required for *en* maintenance and interocellar region specification

en lays both downstream and upstream of the Hh signaling pathway, being activated by Hh and also repressing the pathway

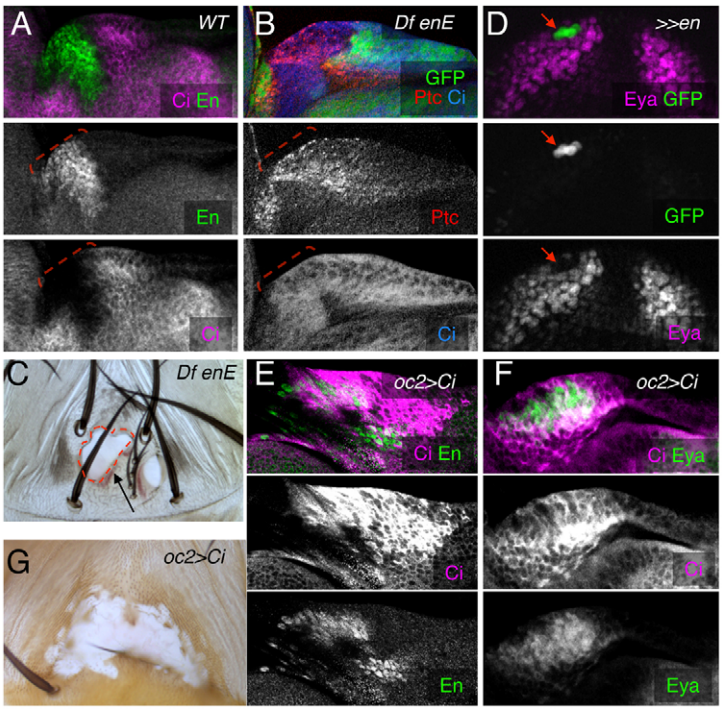

Fig. 3. *en* is a repressor of the *hh* pathway that is required for the interocellar region. (A,B,D-F) Ocellar fields of late-L3 larvae and (C,G) adult ocellar regions. (**A**) Wild-type ocellar field stained for En and Ci. The expression patterns of En and Ci are mutually exclusive. (**B**) A *DfenE* clone spanning the ocellar region. Within the mutant tissue (marked by the absence of GFP), Ptc and Ci are now expressed. The broken lines in A,B mark the approximate span of the En domain in a wild-type disc. (**C**) Ocellar region of an adult containing unmarked *DfenE* clones. A single ocellus extends over the whole left region (arrow). (**D**) Small *en*-expressing clone (>>en), marked with GFP, represses Eya cell-autonomously (arrows). (**E**,**F**) Ocellar fields from *oc2>ci* larvae express high levels of Ci (magenta). Both En (E) and Eya (F) are expressed in a single domain. In all immunofluorescence images, merged and separate channels are shown. (**G**) Ocellar region of a *oc2>ci* adult showing the enlargement of the ocelli and absence of interocellar cuticle. The fact that in this genotype both *en* and RD genes, such as *eya,* are expressed indicates that RD genes are functionally epistatic over *en*.

components *ci* and *ptc*. Therefore, these genetic relationships should lead to an unstable *en* expression (indeed, this conjecture was confirmed by our mathematical modeling, see below). Therefore, after its induction by *hh* signaling, an additional mechanism was required to stably maintain high levels of *en* expression in a *hh*-independent manner. It had been reported that in individuals mutant for a *Notch* temperature-sensitive (N^{ts}) allele, raised at the restrictive temperature during late larval life, the ocelli fuse (Amin, 2004), generating a 'cyclopic' ocellus similar to that observed in *Df(2R)enE* mosaics. To confirm the involvement of *Notch* signaling in ocellar development, we genetically manipulated several *Notch* pathway components. Ocellar-specific knock-downs of the nuclear transducer *Su(H)* [*Su(H)KD*] and the *Dl* ligand (*Dl KD*), or the overexpression of a dominant-negative form of *mastermind* (*mamDN*), a *Notch* co-activator, resulted in expanded or fused ocelli (Fig. 4A; and not shown). Interestingly, similar knock down of the other *Notch* ligand, *Ser*, does not affect ocellar complex development (not shown). The similarity between the *Notch* pathway mutant phenotypes and the loss of *en* pointed to *Notch* signaling being required for *en* expression. Indeed, in *Su(H)KD* discs, the *en* domain is reduced in size and expression intensity and, concomitantly, the two RD domains extend, contacting each other (Fig. 4B,C).

In principle, the input of *Dl/Notch* in the network could be upstream of *hh* (maintaining its expression or signaling) or parallel to *hh*. However, the incomplete activation of *en* should persist in the former scenario. When we checked the signaling status of the *hh* pathway in *Su(H)KD* discs by analyzing *ptc* expression, we

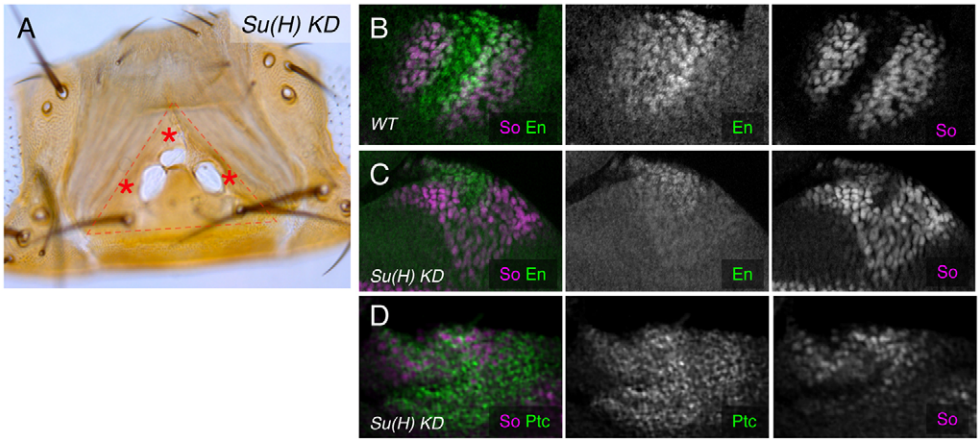

Fig. 4. *Notch* signaling is required for *en* expression and the specification of the interocellar region. (A) Adult dorsal head and (B-D) late-L3 ocellar fields. (**A**) A *oc2>Su(H) RNAi* [*Su(H)KD*] individual, showing enlarged ocelli (asterisks) at the expense of the interocellar region. No interocellar bristles remain. The ocellar complex region is marked by the triangle. (**B**) Wild-type expression of *en* and *so*. (**C**) In *Su(H)KD* discs, the *en* expression domain is weaker and smaller, whereas the *so* domains extend and fuse into a single domain. (**D**) In this genotype, the *hh* signaling pathway is not compromised, as strong Ptc signal is detected throughout the prospective ocellar field.

detected an unsplit domain of strong Ptc signal, indicative of sustained *hh* production and signaling when the activity of the *Notch* pathway is reduced (Fig. 4D). In addition, the fact that knocking down the *Notch* pathway still allowed specification of ocelli, which is a *hh*-controlled fate, agrees with *Dl/Notch* acting parallel to, or downstream of, *hh*.

To determine the developmental window in which *Notch* signaling was required for the maintenance of *en*, we performed the following experiment. *Dl* expression was knocked down at different times during third instar, taking advantage of the temperature sensitivity of the GAL4/UAS system (supplementary material Fig. S1; see also Materials and methods), and the size of the interocellar cuticle in adults was analyzed, the fate of which depends on stable and high levels of *en* expression. Interocellar cuticle surface was estimated by the number of interocellar bristles formed (from 0 in its absence, to 6-8 in the wild type). Disconnecting *Dl/Notch* signaling using a *UAS-Dl-RNAi* (*oc2>Dl-RNAi* or '*Dl KD*') prior to 80 hours post fertilization (hpf) results in almost total absence of interocellar cuticle. *Dl KD* during the 80-85 hpf interval results in intermediate phenotypes with incomplete and variable interocellar regions (supplementary material Fig. S1). Interestingly, this developmental window coincides with the establishment of a strong domain of *en* expression and the split of the *eya*/*so* domain in the disc (not shown). Knocking down *Dl* after 85 hpf no longer precludes the generation of the interocellar cuticle. This result shows that *Notch* signaling activity is required to establish the interocellar fate during a short developmental interval (coinciding with upregulation of *en* in the ocellar field), after which, it remains stable. As the interocellar fate depends on *en*, we interpret this result as *en* expression becoming fixed by *Notch* during the 80-85 hour interval.

A mathematical model for the Hh-driven ocellar patterning

In order to test whether our genetic reasoning was capable of generating the ocellar pattern, we developed a mathematical model incorporating all known genetic interactions (Fig. 5A). Several simplifications were made. First, the two-dimensional ocellar region is modeled as one dimensional (i.e. Fig. 5B, as a row of 31 cells). Second, the *hh* transcription domain (the central five cells) is set as a de facto in our model. Third, our model assumes that there is no proliferation during the developmental interval considered (see supplementary material Appendix S1). Hh production and diffusion have been modeled as in Eqn 1 (see Materials and methods), similar to the formalism used by Nahmad and Stathopoulos to model Hh gradient formation in the wing primordium, considering a diffusion coefficient of $D=0.5\mu m^2/s$ (Nahmad and Stathopoulos, 2009). Downstream of the Hh gradient, transcription and translation of all genes have been modeled using ordinary differential equations (ODEs), essentially following the modeling of the *Drosophila* embryonic segment polarity network by von Dassow and colleagues (von Dassow et al., 2000). Gene transcription may generally be affected by basal (b) and regulated transcription (T), and autoregulation (a), plus a decay term (Fig. 5C). Autoregulation is relevant only for *en* and *eya*. Transcriptional regulation terms have been modeled as sigmoids, allowing for potential cooperativity in transcriptional activation and repression. The general form of the transcription and translation equations, as well as the full set of equations are described in Materials and methods. In what follows, we explain how the new regulatory steps have been modeled. Further details on the specific biology underlying other equations (Eqns 2-7) are

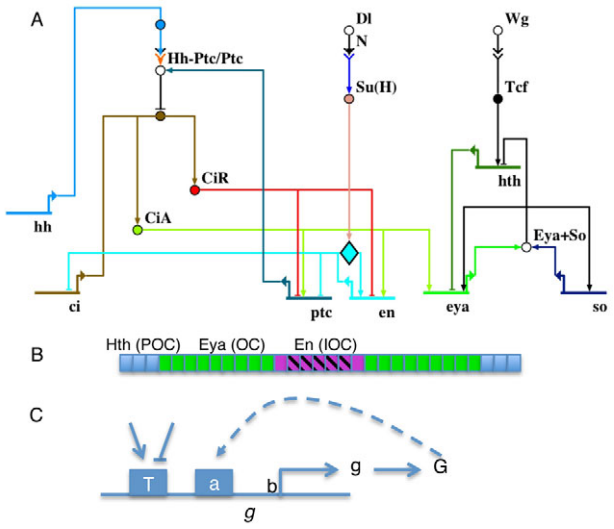

Fig. 5. Regulatory network and one-dimensional model. (**A**) Biotapestry 'view from the genome' of the gene network. (**B**) One-dimensional lattice of 31 cells. *hh* is transcribed in the middle five cells (stripes). The target patterns for Eya (green), En (purple) and Hth (blue) are represented. These patterns correspond to the prospective ocellar (OC), interocellar (IOC) and periocellar (POC) regions. (**C**) Generic gene (*g*) model. Transcript (g) and protein product (G) are indicated. The rate of transcription is dictated by basal transcription rate ('b'), regulated transcription, both positive and negative ('T'), and autoregulation ('a'). Decay rates applying to g and G and have not been represented.

described in supplementary material Appendix S1. We have shown that *Dl*/*Notch* signaling is required for maintaining high En levels in the interocellar region. We have modeled *en* maintenance as an autoregulation (Eqn 8), as *en* has been shown to autoregulate during embryo segmentation (Heemskerk et al., 1991). The contribution of *Dl*/*Notch* signaling would be to facilitate the autoregulation of *en* by lowering *k* in the autoregulatory term (which indicates the En concentration for which half autoregulatory activation is reached). Because of this, it has been named k_{DlEn}. This implementation is the simplest form of representing the role of *Dl/Notch* in allowing *en* autoregulation we could think of. It considers a constant and uniform *Dl/Notch* input and that the *hh* and *Notch* pathway act independently of one another. The *en* autoregulation adds on top of a positive Hh signaling input on *en* transcription (Eqn 8). The expression of *eya* has been shown to depend only on CiA (Blanco et al., 2009), so no CiR input on *eya* regulation has been included. In addition, the *eya-so* positive-feedback loop (Pauli et al., 2005; Brockmann et al., 2011) has been collapsed into a direct *eya* autoregulation for simplicity (Eqn 10). In addition, previous results had suggested a mutual repression between *hth* and *eya* (Brockmann et al., 2011), which is probably direct (supplementary material Fig. S2). Therefore, *hth* has been modeled as a repressor input on *eya* (Eqn 10). In addition, *hth* transcription is modeled as being positively regulated by a constant term (α_{wg}) (Eqn 12), which represents the likely action of Wnt1/*wingless* (*wg*) (Azpiazu and Morata, 2000; Casares and Mann, 2000; Pichaud and Casares, 2000).

The working model has 61 free parameters. For a few, prior biological knowledge is helpful in defining at least some ranges. For example, the basal transcription rates of *ptc* and *ci* are positive, as these genes are widely transcribed. In order to generate a working set of parameter values that result in the target 'wild-type'

pattern (Fig. 5B, seven interocellar and two patches of nine ocellar cells in a 31 row), we first built a one-cell model in which to carry out the first parameter exploration. Then, this parameter set was used as a starting point to manually fine-tune the parameter values on the full model to reach a control pattern (see Materials and methods for further details). With this set of parameter values (supplementary material Table S1), the model accurately recapitulates the target pattern, including the dynamics of Eya, Ptc, CiA, En and Hth expression (Fig. 6; supplementary material Fig. S3). Modeling indicates that before reaching a steady state, the Hh gradient undergoes a transient expansion or 'overshoot' (Fig. 6A,B). This early dynamics depends on the non-linear Ptc-mediated feedback (Casali and Struhl, 2004; Nahmad and Stathopoulos, 2009). The model also predicts observed mutant behaviors, including the expansion of the ocellar tissue at the expense of interocellar cuticle in *Dl* and *en* loss-of-function mutants, or the effects of *hth* on ocellar size (supplementary material Fig. S4). Another computational experiment, the overexpression of *Dl*, predicted the expansion of the interocellar region at the expense of the ocelli. When this prediction was tested experimentally, by overexpressing *Dl* in the developing ocellar region (*oc2>Dl*), the interocellar region enlarged and the anterior ocellus disappeared (supplementary material Fig. S4).

The model GRN is robust against variations in initial conditions and noise

An important test for any systems behavior is the stability of its solution and whether this solution is unique or not. To test this point, the initial condition of every system variable was randomized (up to a 10-fold change) in each individual cell (supplementary material Table S2). The solution obtained for the system is stable, as the resulting patterns are the same as the wild type (supplementary material Fig. S5A). Only when the initial condition for En exceeds the concentration determined by the parameter k_{DlEn}, which is responsible for En autoregulation (k_{DlEn}>0.2), is *en* expression fixed throughout, which precludes the establishment of the *eya* pattern, as expected (supplementary material Fig. 5B,C). In fact, En expression is not detected in the ocellar region until mid-L3, after Eya expression has increased uniformly in the ocellar region (not shown).

Next, and to test whether the network topology is robust to fluctuations, we perturbed all parameters related with production and degradation rates (α_X,θ_X,β_X) with a uniform random signal (white noise). The noise amplitude was 20% for each corresponding rate (Fig. 7A). This fluctuation alters the evolution of the network elements as shown in the Eya time series of Fig. 7B. Under these conditions, the system reproduces the ocellar pattern with a slight deviation (widening) of the interocellar region. This experiment shows that indeed the network model is robust. To further test the robustness of the biological system, we subjected several *Drosophila* strains to temperature fluctuations during early L3, as a means to increase the noise in the system (Li et al., 2009). We included two reference strains as controls (the wild-type strain Oregon-R and w^{1118}) and stocks in which the gene dose of *smo*, *ptc*, *ci* and *Notch* is halved (see Materials and methods), and measured the longer axes of the anterior and posterior ocelli and the interocellar distance. These different genotypes can be thought of as representing the same gene network in which the parameter values may have different, genotype-specific, values. First, we found that different strains showed differences in ocellar and interocellar sizes, indicating that the genotype has a significant influence in the precise size and proportions within the ocellar complex (supplementary material Fig. S6). Second, and directly related to the aim of the experiment, we found that for some genotypes, the temperature fluctuation regime results in size deviations from the control. However, these deviations are smaller than the differences between genotypes. For example, while the difference in ocellar size between w^{1118} and *Notch–/+* (at 25°C) is about 12%, the temperature fluctuations alter ocellar size in *Notch–/+* by only 5%. Furthermore, the external noise introduced did not result in a significantly 'noisier' phenotype, measured as the coefficient of variation of ocellar and interocellar sizes

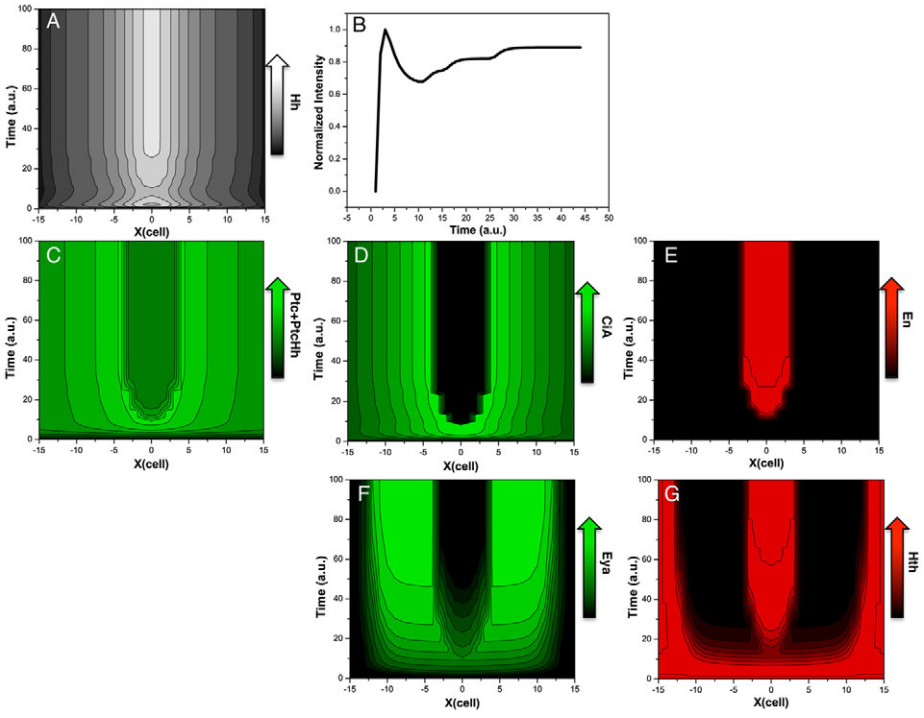

Fig. 6. Spatiotemporal dynamics of the Hh gradient and observed model variables. (**A**) Surface contour plot showing the Hh gradient dynamics. (**B**) Temporal variation of Hh concentration (normalized intensity) in cell 5. The magnitude of the Hh gradient varies with time, with an early 'overshoot', followed by a retraction to then reaching steady state. (**C-G**) Surface contour plots for the wild-type set of parameters depicting the dynamics of the variables that have been experimentally analyzed: total Ptc (Ptc+Ptc:Hh, C), CiA (D), En (E), Eya (F) and Hth (G). With this parameter set, the model correctly predicts qualitatively the biological pattern. (a.u.: arbitrary units). Cell number is represented on the *x* axis.

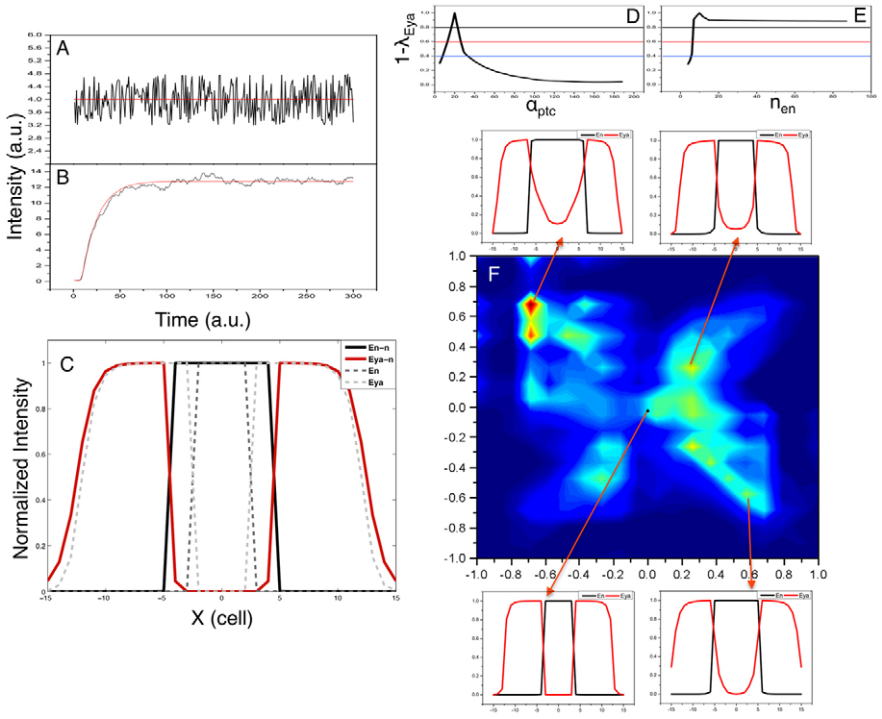

Fig. 7. Analysis of the robustness of the model against noise and parameter variations. (**A**) Application of a white noise distribution of 20% amplitude to θ_{en} as an example of noise implementation. (**B**) Eya time series with- and without-noise rates, shown in black and red. (**C**) Eya (red) and En (black) patterns when applying noise (continuous) or without noise (discontinuous). Rates with noise result in slightly broader interocellar region. (**D**,**E**) Examples of complementary distance when varying each parameter at a time over a range of two orders of magnitude. (D) α_{ptc} presents narrow ranges for 'good', 'medium' and 'bad' patterns [thresholds black (>0.8), red (0.6-0.8) and blue (0.4-0.6), respectively], while (E) n_{en} remains in the 'good' range in most of the studied range. (**F**) Density plot of 10,000 points in the 13-dimensional space corresponding to the distances of the 13 variable patterns to the wild type (black dot, situated at point 0,0). Some Eya and En patterns are also shown corresponding to the wild-type condition (bottom-left diagram) and three additional cases extracted from dense clusters located at different distances from the control.

(supplementary material Fig. S6). Therefore, the ocellar complex is robust against noise, as the model predicts. In addition, different genotypes, equivalent to the same gene network with a (presumably slightly) different set of parameter values, give rise to ocellar patterns that are also quantitatively different, even if these differences are small. The next section explores the properties of the model across the parameter space.

Exploration of parameter space suggests that the network imposes constraints on phenotypic variation

Next, we carried a parameter sensitivity assay. First, and starting with our working parameter set, we varied one parameter at a time in a two orders of magnitude range around its wild-type value, and measured the departure this variation caused from the wild-type pattern. As a metric for this deviation, we calculated a goodness score as a distance (λ) between the wild-type Eya pattern and that obtained from the varied parameter run, both normalized (see supplementary material Appendix S1). We established three thresholds for the complementary of this distance (1-λ): 1-λ≥0.8 ('good'), 0.8>1-λ≥0.6 ('medium') and 0.6>1-λ≥0.4 ('bad'), with 1-λ≥0.8 being the most accurate fits (Fig. 7D,E; supplementary material Table S1). Twenty-eight out of 61 parameters gave goodness values above 0.8 over several orders of magnitude and were classified as 'insensitive' (i.e. large variations in their value did not result in major deviations from the target pattern) (Fig. 7E; supplementary material Fig. S9.1-9.4; supplementary material Table S1). The remaining ones (33) were sensitive (Fig. 7D), although the range of values for each specific parameter that resulted in a score of at least 0.8 varied among them (see supplementary material Table S1). The most sensitive parameter is the basal transcription rate constant α_{en}, which is also the parameter that does not allow variation in the noise experiments. This suggests that *en* expression has to be kept strictly off in the absence of patterned Hh signal. Not surprisingly, other sensitive parameters are those related to *ptc* and *ci* expression, which affect the major feedbacks in the network (supplementary material Table S1).

Second, we carried out an analysis in which all 33 sensitive parameters were simultaneously randomized at each run inside one of the goodness intervals (the remaining parameters were left fixed at their wild-type values). A total of 10,000 runs were obtained, distributed among 'good' (6000), 'medium' (3000) and 'bad' (1000) randomized parameter values. For all 10,000 parameter sets, the distance for all the patterns of the system (one per variable) to the wild type was calculated. In this way, each parameter set defines a point in a 13-dimensional space, each dimension being one of the model variables (see supplementary material Appendix S1). For visualization, this information was reduced to three dimensions, two of them being the projections of the distance distributions two by two, and another representing the density of multidimensional points in such projections. The resulting 2D histogram (Fig. 7F; supplementary material Fig. S7) plots the density of patterns from the 10,000 randomized runs distributed relative to their distance from the wild type (point 0,0) (see supplementary material Appendix S1 for details). Therefore, it represents a map of the phenotypic space generated by the GRN (gene regulatory network) using randomized sets of parameters. Several conclusions can be derived from this analysis. First, the distribution of solutions (patterns) was not evenly dispersed. Instead, the solutions tended to concentrate in clusters or 'islands'. Second, the wild-type pattern was placed inside a big and dense cluster, so this solution is highly probable, which indicates that the pattern is stable. Finally, when we analyzed the patterns of Eya and En (the two major readouts of the GRN) located in dense islands far apart from the wild type, we found that those patterns were still qualitatively similar to the wild type [Fig. 7F; see, for example, the high stability island around (−0.7,0.7) in supplementary material Fig. S7B]. This is interesting, because in this experiment we used parameter values coming not only from the 'good' interval, but also from 'medium' and 'bad' ones, as derived from our previous single parameter analysis. In summary, these analyses indicate that the

GRN is robust, because wide and random parameter variation results in specific phenotypic clusters, all of them similar to the wild type.

DISCUSSION

Many gene networks are described as static regulatory (activating and inhibitory) relationships between network components (genes and their products), disregarding essential dynamic and spatial aspects. In such descriptions, all genetic interactions are given as though happening at once and without spatial context. Mathematical modeling allows us to test the logic consistency of such networks, and whether or not they are capable of explaining the spatial and temporal dynamics of the biological system.

Using an integration of experimentation and mathematical network modeling, our results help to explain how several alternative fates are controlled by the Hh morphogen (Fig. 8). Previous descriptions of the genetic interactions involved in the specification and patterning of the ocellar complex structures did not offer satisfactory explanations for this fate choice decision.

A first important point is the addition to the GRN of *en* as a *hh* target with self-maintaining capability. The transduction of the Hh gradient generates an initial asymmetry, with only the cells receiving the highest Hh concentrations being able to maintain *en* expression. This in turn sets in motion the dynamics of the GRN. The evolution of some key system components is shown in Fig. 8.

A second important point is the action of *en* as a Hh-pathway repressor. The fact that *en* expression is sustained just in cells receiving the highest Hh concentrations (the Hh-producing cells and their adjacent neighbors) makes these cells read the Hh signal only transiently, as the signaling pathway is blocked as *en* expression builds up. This means that it would be impossible for *en* to reach sufficient expression levels to shut off the pathway – and therefore, to inactivate *eya* – unless additional mechanisms were considered. In fact, the inactivation of *eya* is necessary for the specification of the interocellar region: thus, uniform and high *ci* expression results in the co-expression of *eya* and *en* throughout the ocellar field. In this situation, *eya* is functionally epistatic over *en*, and the only tissue type specified is ocellus. Therefore, a stable interocellar region can be established only if the initiation of *en* expression is followed by a *hh* signaling-independent phase. Such a transition from signal-induced expression to independent mode of maintenance has been reported for *en* during *Drosophila* embryonic segmentation (Heemskerk et al., 1991). In the ocellar field, we propose that this transition requires *Notch* signaling, specifically activated by its ligand *Dl* (but not by *Ser*). The molecular mechanisms of this *en* maintenance are not yet clear, but might involve PREs (polycomb response elements) in the *en* locus (Kwon et al., 2009).

Our model includes another repressor, *hth*, which enters the network as a direct repressor of RD. Its contribution seems limited to restricting the external extent of the *eya*/*so* expression domain. In *hthKD* animals, the ocelli are larger, but the interocellar cuticle is still present. In our model, *en* repressive action suffices to turn off *hh* signaling pathway, thereby precluding RD activation. We have tested, through modeling, the possibility of *hth* being required for *en* activity, as it has been shown to be the case during embryonic segmentation (Kobayashi et al., 2003). In this case, though, making the repression function of *en* dependent on *hth* does not allow the network to reach any steady state in which the interocellar domain is established – i.e. *en* does not reach the maintenance threshold. To verify this prediction, we checked *en* expression and the activity status of the *hh* pathway in *hthKD* discs. As predicted, *en* is expressed at normal levels in a domain where *ci* is off, as in wild type (supplementary material Fig. S8).

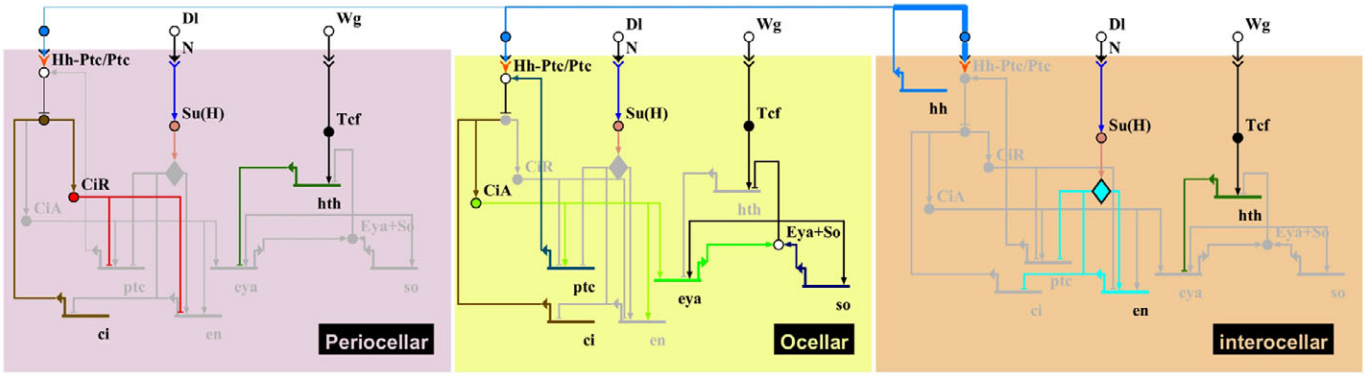

Fig. 8. Logic of the ocellar complex GRN. A Biotapestry representation of the ocellar complex (OC) GRN architecture. Genes are represented by horizontal lines topped by a bent arrow (the transcriptional start site, TSS). Positive and negative interactions (lines emerging from the TSS) are represented by arrows or capped lines, respectively. Protein-protein interactions are represented by circles. Different cell types are symbolized with colored boxes (named accordingly). Cell signaling is represented by lines reaching from inside one cell type to the outside (thickness indicates strength of the signaling); chevrons and circles are used to represent signal reception and transduction, respectively. White circles outside cell boxes represent signaling ligands. Genes and interactions are represented in color if active, in gray otherwise. Three cell types are specified according to the decreasing level of Hh signal they receive: inter-ocellar, ocellar and periocellar cells. Hh signal triggers both RD genes (*eya* and *so*) and *en* expression. In interocellar cells, high Hh concentrations promote the expression of *en*, which in turn represses RD genes by shutting down *ptc* and *ci* expression, and therefore eliminating Hh signal reception. Inside ocellar cells, *en* expression does not occur because of weaker Hh signaling; this makes RD gene activation possible. Ocellar and interocellar cells therefore achieve distinct gene expression patterns. In interocellar cells, *en* expression is maintained by the *Dl*/*Notch* pathway (present throughout the entire OC). This particular interaction is represented with a diamond (within the *en* auto-activation line). RD genes expression domain is also defined through the contribution of *hth*; this gene is likely to be activated downstream of the *wg* pathway. In ocellar cells, Eya and So (acting as a complex) repress *hth*. Periocellar cells lie at the periphery of Hh signaling and RD gene activation is prevented by Hth: this repression contributes to define the size of the ocelli. The periocellar region gives rise to the front cuticle in the adult head.

Recently, a similar situation to the one we detailed here has been described during the dorsoventral patterning of the vertebrate neural tube by *Shh* (Ribes et al., 2010). The floor plate (FP), the ventral-most region of the neural tube, expresses *Shh* and requires maximal *Shh* concentrations for its specification (Chiang et al., 1996; Ericson et al., 1996). However, this requirement is transient and followed by an attenuation of the pathway. This attenuation is necessary for FP specification (Ribes et al., 2010). This process of FP specification is reminiscent of the specification of the interocellar cuticle in our system. This similarity raises the possibility that a negative-feedback loop in the *Shh* pathway, of the type we have described here, could be part of the neural tube GRN. However, after the initial asymmetry within the ocellar field has been established, an external input, the *Dl*/*Notch* signal, is needed to maintain it. In our model, there is no need for a localized *Notch* signal: uniform signaling suffices, provided that *en* expression reaches a specific concentration threshold. In fact, using an anti-*Dl* monoclonal antibody, we detect uniform levels of *Dl* expression in the ocellar field in mid-L3 (not shown), the developmental period when we start to see the distinct domains emerging. Interestingly, a recent report finds an association between mutations in *Dll1,* a vertebrate *Dl*-like ligand, and holoprosencephaly (Dupé et al., 2011). Holoprosencephaly, a developmental defect caused by abnormal specification of the ventral midline structures of the anterior neural tube, is frequently associated with malfunction of the Shh pathway. In fact, work in vertebrates indicates that *Notch* signaling is indeed required for FP fate acquisition parallel to *Shh* (le Roux et al., 2003; Peyrot et al., 2011). It is therefore tempting to speculate that the *Notch* pathway is required to fix the FP fate in the vertebrate neural tube by stabilizing gene expression during the phase of *Shh* signaling attenuation, as we propose here for *Notch* in the *Drosophila* ocellar GRN.

The model we have described explains how mutually exclusive gene expression domains are produced under the control of a Hh gradient by connecting a repressive gene circuitry. These expression domains underlie the morphology of the structures that will later form and cannot be explained unless the information of Hh gradient is integrated with the logic of the GRN. They can therefore be considered as the emerging properties of the system we have described.

The structure of this GRN confers robustness to the patterning mechanism, buffering variations in the initial conditions, as well as absorbing noise. Although the model predicts an early overshoot of the Hh gradient, this might not be crucial, as variations in the initial conditions converge to the same pattern.

Interestingly, random variation of parameter values results in the system deviating from the 'wild-type' pattern in a non-random manner, but instead falling into specific 'islands' of the phenotypic space. That is, variations in the control parameters of the GRN generate phenotypes that maintain certain rules of proportionality. Still these phenotypic 'variants' are robust against noise, as is the wild-type pattern (supplementary material Fig. S7). These mathematical properties of the ocellar network might ensure the phenotypic stability of the ocellar structures in wild flies exposed to varying environmental conditions during development, as well as constraining the phenotypic variability of the ocelli during evolution.

Acknowledgements
We thank I. Guerrero, I. Rebay and R. S. Mann for antibodies; P. Rojas, J. Blanco, C. M. Luque, the Bloomington, VDRC and Flytrap Stock Centers, and the Consolider 'From Genes to Shape' *Drosophila* Collection for fly strains; and O. Abreu for help with experiments.

Funding
This work was funded by the Spanish Ministry for Science and Innovation (MICINN/MINECO, co-funded by Feder program) [BFU2009-07044], by Proyecto de Excelencia CVI 2658 (Junta de Andalucía) to F.C., by Consolider 'From Genes to Shape' (in which F.C. is participant researcher; MICINN/MINECO), and by MICINN/MINECO [FIS2008-04120 to A.C. and M.C.L.].

Competing interests statement
The authors declare no competing financial interests.

Supplementary material
Supplementary material available online at
http://dev.biologists.org/lookup/suppl/doi:10.1242/dev.082172/-/DC1

References

Alexandre, C., Jacinto, A. and Ingham, P. W. (1996). Transcriptional activation of hedgehog target genes in Drosophila is mediated directly by the cubitus interruptus protein, a member of the GLI family of zinc finger DNA-binding proteins. *Genes Dev.* **10**, 2003-2013.
Amin, A. (2004). Genetic cross-talk during head development in Drosophila. *J. Biomed. Biotechnol.* **2004**, 16-23.
Aza-Blanc, P., Ramírez-Weber, F. A., Laget, M. P., Schwartz, C. and Kornberg, T. B. (1997). Proteolysis that is inhibited by hedgehog targets Cubitus interruptus protein to the nucleus and converts it to a repressor. *Cell* **89**, 1043-1053.
Azpiazu, N. and Morata, G. (2000). Function and regulation of homothorax in the wing imaginal disc of Drosophila. *Development* **127**, 2685-2693.
Balaskas, N., Ribeiro, A., Panovska, J., Dessaud, E., Sasai, N., Page, K. M., Briscoe, J. and Ribes, V. (2012). Gene regulatory logic for reading the Sonic Hedgehog signaling gradient in the vertebrate neural tube. *Cell* **148**, 273-284.
Basler, K. and Struhl, G. (1994). Compartment boundaries and the control of Drosophila limb pattern by hedgehog protein. *Nature* **368**, 208-214.
Bessa, J. and Casares, F. (2005). Restricted teashirt expression confers eye-specific responsiveness to Dpp and Wg signals during eye specification in Drosophila. *Development* **132**, 5011-5020.
Biehs, B., Kechris, K., Liu, S. and Kornberg, T. B. (2010). Hedgehog targets in the Drosophila embryo and the mechanisms that generate tissue-specific outputs of Hedgehog signaling. *Development* **137**, 3887-3898.
Blanco, J., Seimiya, M., Pauli, T., Reichert, H. and Gehring, W. J. (2009). Wingless and Hedgehog signaling pathways regulate orthodenticle and eyes absent during ocelli development in Drosophila. *Dev. Biol.* **329**, 104-115.
Blanco, J., Pauli, T., Seimiya, M., Udolph, G. and Gehring, W. J. (2010). Genetic interactions of eyes absent, twin of eyeless and orthodenticle regulate sine oculis expression during ocellar development in Drosophila. *Dev. Biol.* **344**, 1088-1099.
Bonini, N. M., Leiserson, W. M. and Benzer, S. (1993). The eyes absent gene: genetic control of cell survival and differentiation in the developing Drosophila eye. *Cell* **72**, 379-395.
Bonini, N. M., Leiserson, W. M. and Benzer, S. (1998). Multiple roles of the eyes absent gene in Drosophila. *Dev. Biol.* **196**, 42-57.
Briscoe, J., Chen, Y., Jessell, T. M. and Struhl, G. (2001). A hedgehog-insensitive form of patched provides evidence for direct long-range morphogen activity of sonic hedgehog in the neural tube. *Mol. Cell* **7**, 1279-1291.
Brockmann, A., Domínguez-Cejudo, M. A., Amore, G. and Casares, F. (2011). Regulation of ocellar specification and size by twin of eyeless and homothorax. *Dev. Dyn.* **240**, 75-85.
Buszczak, M., Paterno, S., Lighthouse, D., Bachman, J., Planck, J., Owen, S., Skora, A. D., Nystul, T. G., Ohlstein, B., Allen, A. et al. (2007). The carnegie protein trap library: a versatile tool for Drosophila developmental studies. *Genetics* **175**, 1505-1531.
Casali, A. and Struhl, G. (2004). Reading the Hedgehog morphogen gradient by measuring the ratio of bound to unbound Patched protein. *Nature* **431**, 76-80.
Casares, F. and Mann, R. S. (2000). A dual role for homothorax in inhibiting wing blade development and specifying proximal wing identities in Drosophila. *Development* **127**, 1499-1508.
Chen, Y. and Struhl, G. (1996). Dual roles for patched in sequestering and transducing Hedgehog. *Cell* **87**, 553-563.
Cheyette, B. N., Green, P. J., Martin, K., Garren, H., Hartenstein, V. and Zipursky, S. L. (1994). The Drosophila sine oculis locus encodes a homeodomain-containing protein required for the development of the entire visual system. *Neuron* **12**, 977-996.
Chiang, C., Litingtung, Y., Lee, E., Young, K. E., Corden, J. L., Westphal, H. and Beachy, P. A. (1996). Cyclopia and defective axial patterning in mice lacking Sonic hedgehog gene function. *Nature* **383**, 407-413.
Davidson, E. H. (2006) *The Regulatory Genome: Gene Regulatory Networks in Development and Evolution.* San Diego, CA: Academic Press.
Dessaud, E., Yang, L. L., Hill, K., Cox, B., Ulloa, F., Ribeiro, A., Mynett, A., Novitch, B. G. and Briscoe, J. (2007). Interpretation of the sonic hedgehog

morphogen gradient by a temporal adaptation mechanism. *Nature* **450**, 717-720.
Dessaud, E., McMahon, A. P. and Briscoe, J. (2008). Pattern formation in the vertebrate neural tube: a sonic hedgehog morphogen-regulated transcriptional network. *Development* **135**, 2489-2503.
Dessaud, E., Ribes, V., Balaskas, N., Yang, L. L., Pierani, A., Kicheva, A., Novitch, B. G., Briscoe, J. and Sasai, N. (2010). Dynamic assignment and maintenance of positional identity in the ventral neural tube by the morphogen sonic hedgehog. *PLoS Biol.* **8**, e1000382.
Domínguez, M., Brunner, M., Hafen, E. and Basler, K. (1996). Sending and receiving the hedgehog signal: control by the Drosophila Gli protein Cubitus interruptus. *Science* **272**, 1621-1625.
Dupé, V., Rochard, L., Mercier, S., Le Pétillon, Y., Gicquel, I., Bendavid, C., Bourrouillou, G., Kini, U., Thauvin-Robinet, C., Bohan, T. P. et al. (2011). NOTCH, a new signaling pathway implicated in holoprosencephaly. *Hum. Mol. Genet.* **20**, 1122-1131.
Eaton, S. and Kornberg, T. B. (1990). Repression of ci-D in posterior compartments of Drosophila by engrailed. *Genes Dev.* **4**, 1068-1077.
Ericson, J., Morton, S., Kawakami, A., Roelink, H. and Jessell, T. M. (1996). Two critical periods of Sonic Hedgehog signaling required for the specification of motor neuron identity. *Cell* **87**, 661-673.
Finkelstein, R., Smouse, D., Capaci, T. M., Spradling, A. C. and Perrimon, N. (1990). The orthodenticle gene encodes a novel homeo domain protein involved in the development of the Drosophila nervous system and ocellar visual structures. *Genes Dev.* **4**, 1516-1527.
Freeman, M. and Gurdon, J. B. (2002). Regulatory principles of developmental signaling. *Annu. Rev. Cell Dev. Biol.* **18**, 515-539.
González, A., Chaouiya, C. and Thieffry, D. (2008). Logical modelling of the role of the Hh pathway in the patterning of the Drosophila wing disc. *Bioinformatics* **24**, i234-i240.
Guillén, I., Mullor, J. L., Capdevila, J., Sánchez-Herrero, E., Morata, G. and Guerrero, I. (1995). The function of engrailed and the specification of Drosophila wing pattern. *Development* **121**, 3447-3456.
Haynie, J. L. and Bryant, P. J. (1986). Development of the eye-antenna imaginal disc and morphogenesis of the adult head in Drosophila melanogaster. *J. Exp. Zool.* **237**, 293-308.
Heemskerk, J., DiNardo, S., Kostriken, R. and O'Farrell, P. H. (1991). Multiple modes of engrailed regulation in the progression towards cell fate determination. *Nature* **352**, 404-410.
Hidalgo, A. and Ingham, P. (1990). Cell patterning in the Drosophila segment: spatial regulation of the segment polarity gene patched. *Development* **110**, 291-301.
Ingham, P. W., Nakano, Y. and Seger, C. (2011). Mechanisms and functions of Hedgehog signalling across the metazoa. *Nat. Rev. Genet.* **12**, 393-406.
Irons, D. J., Wojcinski, A., Glise, B. and Monk, N. A. (2010). Robustness of positional specification by the Hedgehog morphogen gradient. *Dev. Biol.* **342**, 180-193.
Jaynes, J. B. and O'Farrell, P. H. (1991). Active repression of transcription by the engrailed homeodomain protein. *EMBO J.* **10**, 1427-1433.
Jiang, J. and Hui, C. C. (2008). Hedgehog signaling in development and cancer. *Dev. Cell* **15**, 801-812.
Kobayashi, M., Fujioka, M., Tolkunova, E. N., Deka, D., Abu-Shaar, M., Mann, R. S. and Jaynes, J. B. (2003). Engrailed cooperates with extradenticle and homothorax to repress target genes in Drosophila. *Development* **130**, 741-751.
Kumar, J. P. and Moses, K. (2001). EGF receptor and Notch signaling act upstream of Eyeless/Pax6 to control eye specification. *Cell* **104**, 687-697.
Kwon, D., Mucci, D., Langlais, K. K., Americo, J. L., DeVido, S. K., Cheng, Y. and Kassis, J. A. (2009). Enhancer-promoter communication at the Drosophila engrailed locus. *Development* **136**, 3067-3075.
le Roux, I., Lewis, J. and Ish-Horowicz, D. (2003). Notch activity is required to maintain floorplate identity and to control neurogenesis in the chick hindbrain and spinal cord. *Int. J. Dev. Biol.* **47**, 263-272.
Li, X., Cassidy, J. J., Reinke, C. A., Fischboeck, S. and Carthew, R. W. (2009). A microRNA imparts robustness against environmental fluctuation during development. *Cell* **137**, 273-282.
Marigo, V. and Tabin, C. J. (1996). Regulation of patched by sonic hedgehog in the developing neural tube. *Proc. Natl. Acad. Sci. USA* **93**, 9346-9351.
Méthot, N. and Basler, K. (1999). Hedgehog controls limb development by regulating the activities of distinct transcriptional activator and repressor forms of Cubitus interruptus. *Cell* **96**, 819-831.
Mutsuddi, M., Chaffee, B., Cassidy, J., Silver, S. J., Tootle, T. L. and Rebay, I. (2005). Using Drosophila to decipher how mutations associated with human branchio-oto-renal syndrome and optical defects compromise the protein tyrosine phosphatase and transcriptional functions of eyes absent. *Genetics* **170**, 687-695.
Nahmad, M. and Stathopoulos, A. (2009). Dynamic interpretation of hedgehog signaling in the Drosophila wing disc. *PLoS Biol.* **7**, e1000202.
Nakano, Y., Guerrero, I., Hidalgo, A., Taylor, A., Whittle, J. R. and Ingham, P. W. (1989). A protein with several possible membrane-spanning domains encoded by the Drosophila segment polarity gene patched. *Nature* **341**, 508-513.
Ohlmeyer, J. T. and Kalderon, D. (1998). Hedgehog stimulates maturation of Cubitus interruptus into a labile transcriptional activator. *Nature* **396**, 749-753.
Pauli, T., Seimiya, M., Blanco, J. and Gehring, W. J. (2005). Identification of functional sine oculis motifs in the autoregulatory element of its own gene, in the eyeless enhancer and in the signalling gene hedgehog. *Development* **132**, 2771-2782.
Peyrot, S. M., Wallingford, J. B. and Harland, R. M. (2011). A revised model of Xenopus dorsal midline development: differential and separable requirements for Notch and Shh signaling. *Dev. Biol.* **352**, 254-266.
Pichaud, F. and Casares, F. (2000). homothorax and iroquois-C genes are required for the establishment of territories within the developing eye disc. *Mech. Dev.* **96**, 15-25.
Probst, S., Kraemer, C., Demougin, P., Sheth, R., Martin, G. R., Shiratori, H., Hamada, H., Iber, D., Zeller, R. and Zuniga, A. (2011). SHH propagates distal limb bud development by enhancing CYP26B1-mediated retinoic acid clearance via AER-FGF signalling. *Development* **138**, 1913-1923.
Punzo, C., Seimiya, M., Flister, S., Gehring, W. J. and Plaza, S. (2002). Differential interactions of eyeless and twin of eyeless with the sine oculis enhancer. *Development* **129**, 625-634.
Ribes, V., Balaskas, N., Sasai, N., Cruz, C., Dessaud, E., Cayuso, J., Tozer, S., Yang, L. L., Novitch, B., Marti, E. et al. (2010). Distinct Sonic Hedgehog signaling dynamics specify floor plate and ventral neuronal progenitors in the vertebrate neural tube. *Genes Dev.* **24**, 1186-1200.
Royet, J. and Finkelstein, R. (1995). Pattern formation in Drosophila head development: the role of the orthodenticle homeobox gene. *Development* **121**, 3561-3572.
Royet, J. and Finkelstein, R. (1996). hedgehog, wingless and orthodenticle specify adult head development in Drosophila. *Development* **122**, 1849-1858.
Royet, J. and Finkelstein, R. (1997). Establishing primordia in the Drosophila eye-antennal imaginal disc: the roles of decapentaplegic, wingless and hedgehog. *Development* **124**, 4793-4800.
Saha, K. and Schaffer, D. V. (2006). Signal dynamics in Sonic hedgehog tissue patterning. *Development* **133**, 889-900.
Sanicola, M., Sekelsky, J., Elson, S. and Gelbart, W. M. (1995). Drawing a stripe in Drosophila imaginal disks: negative regulation of decapentaplegic and patched expression by engrailed. *Genetics* **139**, 745-756.
Schwartz, C., Locke, J., Nishida, C. and Kornberg, T. B. (1995). Analysis of cubitus interruptus regulation in Drosophila embryos and imaginal disks. *Development* **121**, 1625-1635.
Serikaku, M. A. and O'Tousa, J. E. (1994). Sine oculis is a homeobox gene required for Drosophila visual system development, *Genetics* **138**. 1137-1150.
Tabata, T., Schwartz, C., Gustavson, E., Ali, Z. and Kornberg, T. B. (1995). Creating a Drosophila wing de novo, the role of engrailed, and the compartment border hypothesis. *Development* **121**, 3359-3369.
Varjosalo, M. and Taipale, J. (2008). Hedgehog: functions and mechanisms. *Genes Dev.* **22**, 2454-2472.
von Dassow, G., Meir, E., Munro, E. M. and Odell, G. M. (2000). The segment polarity network is a robust developmental module. *Nature* **406**, 188-192.
Wang, L. H., Huang, Y. T., Tsai, Y. C. and Sun, Y. H. (2010). The role of eyg Pax gene in the development of the head vertex in Drosophila. *Dev. Biol.* **337**, 246-258.
Wieschaus, E., Perrimon, N. and Finkelstein, R. (1992). orthodenticle activity is required for the development of medial structures in the larval and adult epidermis of Drosophila. *Development* **115**, 801-811.
Xu, T. and Rubin, G. M. (1993). Analysis of genetic mosaics in developing and adult Drosophila tissues. *Development* **117**, 1223-1237.

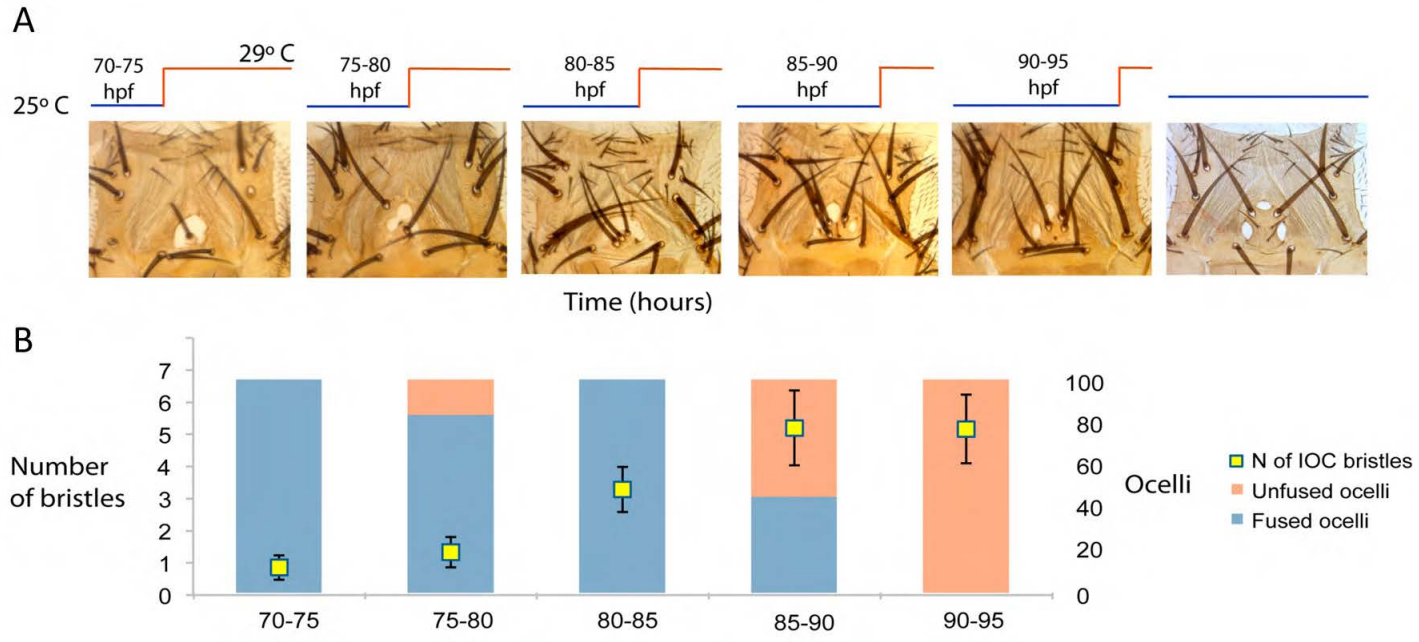

Fig. S1. Temporal requirement of *Dl/Notch* signaling for interocellar fate establishment. (**A**) Five-hour collections of *oc2>Dl-RNAi* embryos were grown at 25°C and shifted to 29°C at different developmental times as indicated. Representative views of the ocellar complex are shown. Maintenance of the culture at 25°C results in wild-type flies (last panel). Shifted animals develop macrobristles in the interocellar region, instead of the normal microbristles in the wild type. This is probably due to precocious bristle differentiation in the absence of *Dl* signaling, independent of the earlier role in interocellar fate specification of *Dl*. (**B**) Quantification of the number of interocellar bristles (yellow squares with standard error bars). Rectangles represent the percentage of flies with fused (cyclopic) and unfused ocelli. After 85 hpf, the interocellar region becomes *Dl/Notch* independent.

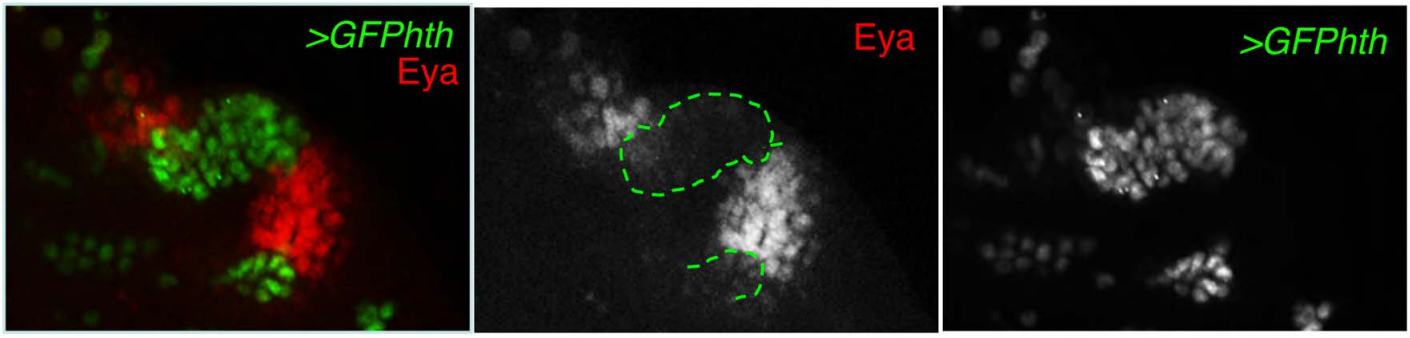

Fig. S2. *hth* represses Eya cell-autonomously. *GFPhth*-expressing clones (green) in the ocellar field, stained for Eya expression. Merged and single channels are shown. *GFPhth* represses *eya* expression cell autonomously. The clones are outlined on the Eya channel.

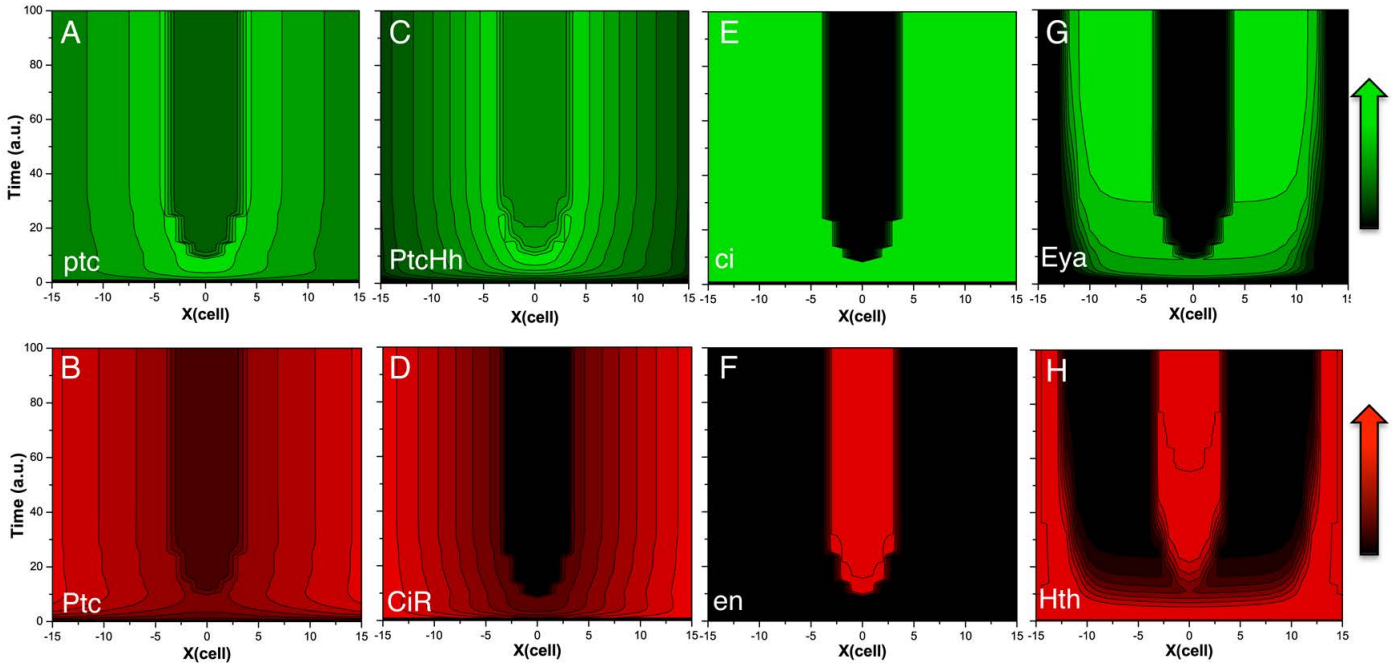

Fig. S3. Spatiotemporal dynamics of model variables. Surface contour plots showing the spatiotemporal patterns of model variables not described in Fig. 6. Capitalized names indicate protein products, whereas non-capitalized names indicate transcript species. a.u., arbitrary units. Cell number is represented on the *x* axis.

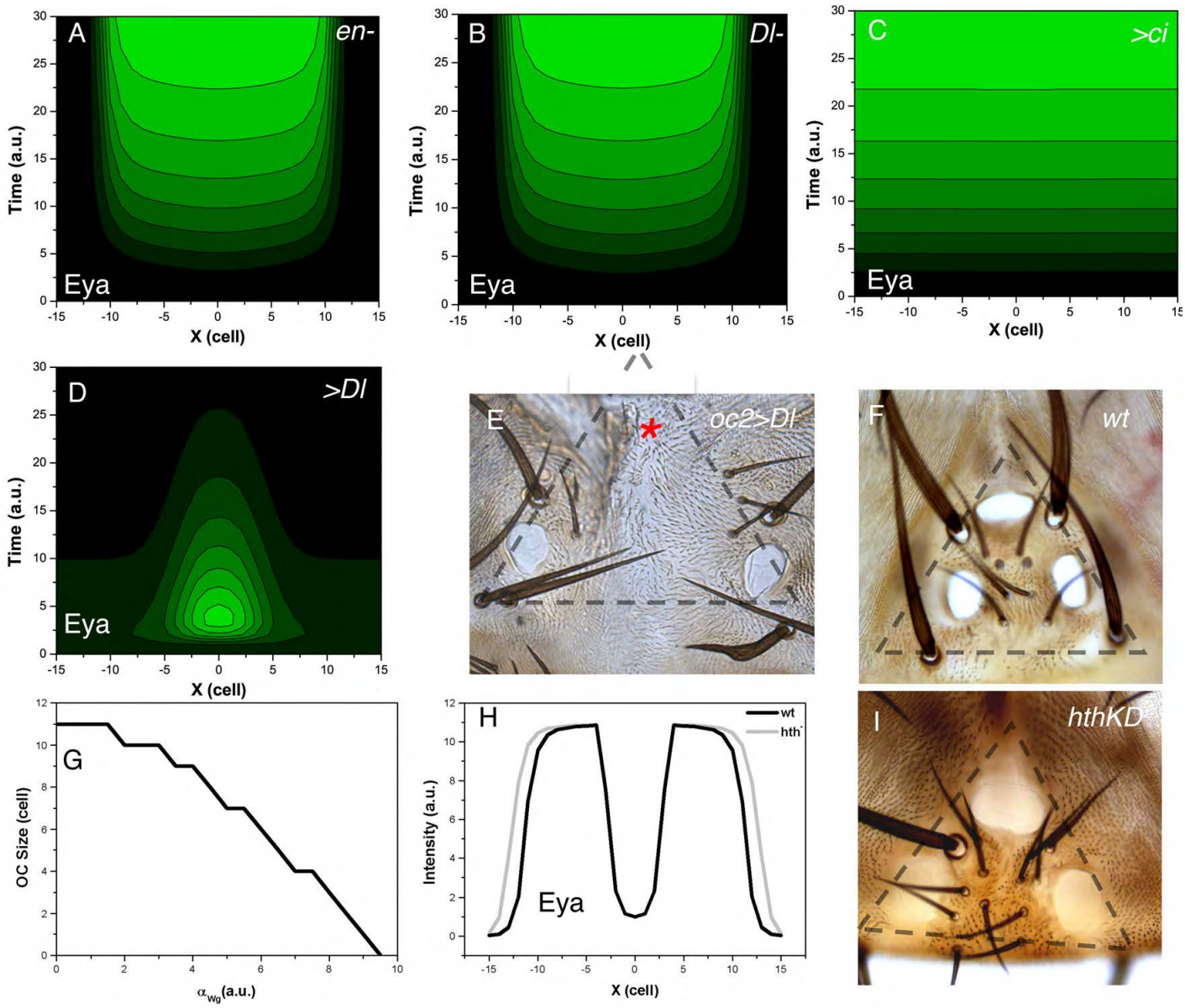

Fig. S4. Analaysis of mutant genotypes. (**A-D**) Spatiotemporal dynamics of Eya expression predicted in modeled mutants, as indicated in each panel. To mimic loss of function mutations in *en*, *Dl* and *hth*, the following parameters values were used: θ_{en}=0; k_{DlEn}=2; α_{Wghth}=0, respectively. The overexpression of *ci* and *Dl* were modeled by increasing the *ci* basal transcription rate (α_{ci}=6) and by reducing k_{DlEn} (k_{DlEn}=0.1), respectively. Simulations of *en* (A) and *Dl* (B) loss reproduce qualitatively the results shown in Fig. 3C and Fig. 4A,C (expansion of the ocellar/Eya domain and loss of the interocellar region). Overexpression of *ci* (C) results in extended Eya-positive/ocellar tissue, as observed experimentally in Fig. 3G. *Dl* overexpression is predicted to expand the interocellar region at the expense of the Eya-expressing domains (D) (and thereby the ocelli) which, with the parameters used, result in the loss of ocelli. (**E**,**F**) When this prediction is tested in vivo by overexpression of *Dl* driven by *oc2-GAL4* (*oc2>Dl*), the interocellar region expands notably and the anterior ocellus disapears (asterisk). The posterior ocelli are abnormally shaped, but still present (E), suggesting uneven expression of the *oc2-GAL4* driver in the ocellar region or unrecognized biological asymmetries between anterior and posterior ocelli. (**G**) The expression of *hth* is predicted to regulate the size of the ocellar domain, such that as its transcription increases (i.e. increasing α_{Wg}) the ocellar domain (the number of Eya-expressing cells) decreases. (**H**) Therefore, when *hth* transcription is shut off, the Eya domain expands. (**I**) This is indeed what is detected by knocking down in vivo *hth* expression, in *oc2>hthRNAi* ('*hthKD*') individuals. Note the irregular perimeter of the ocelli in this genotype. a.u., arbitrary units.

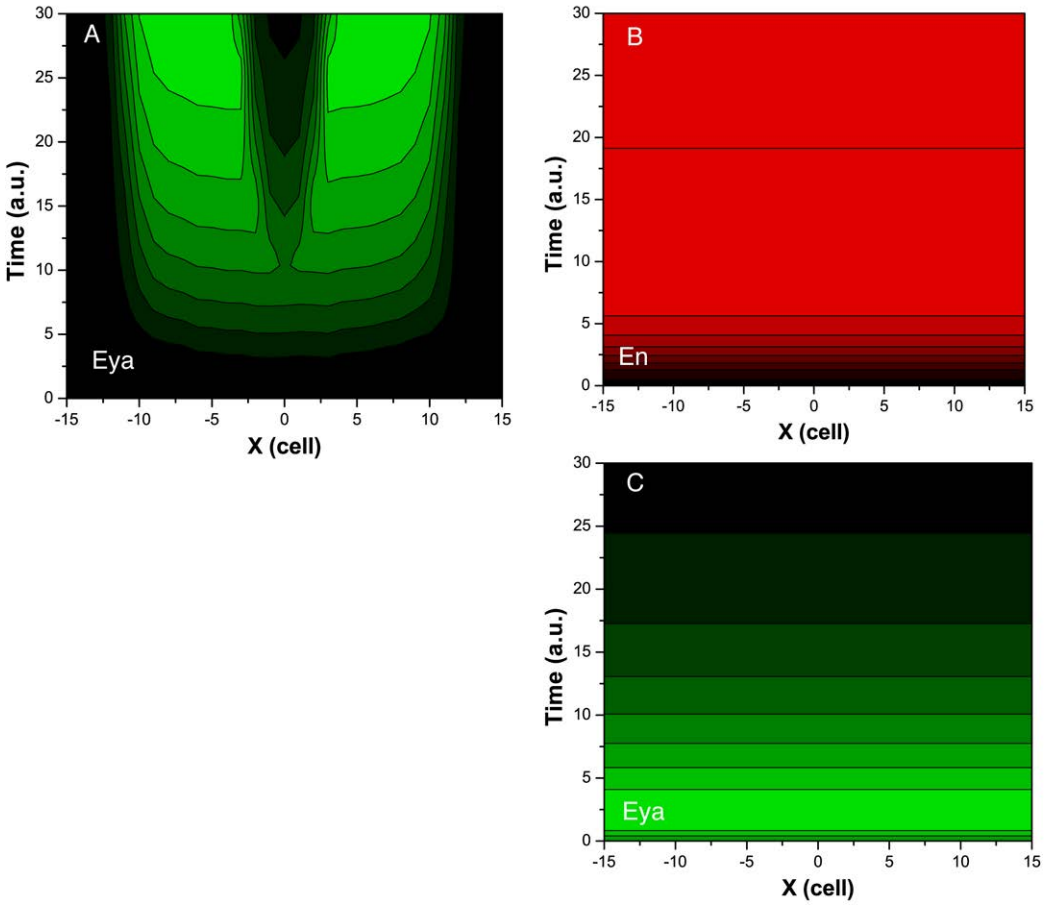

Fig. S5. Convergence to the wild-type pattern with varying initial conditions. Surface contour plots showing the spatiotemporal patterns of model variables. (**A**) Evolution of Eya pattern when the initial value of every system variable was randomized (up to a 10-fold change) in each individual cell. The different initial conditions applied to each cell describe a fluctuating spatiotemporal pattern in the first time steps. These fluctuations are smoothed with time as the system converges to a stable stationary solution. (**B**,**C**) Evolution of En (B) and Eya (C) when the initial condition for En exceeds the concentration determined by the parameter k_{DlEn}, responsible for En autoregulation (k_{DlEn}>0.2).

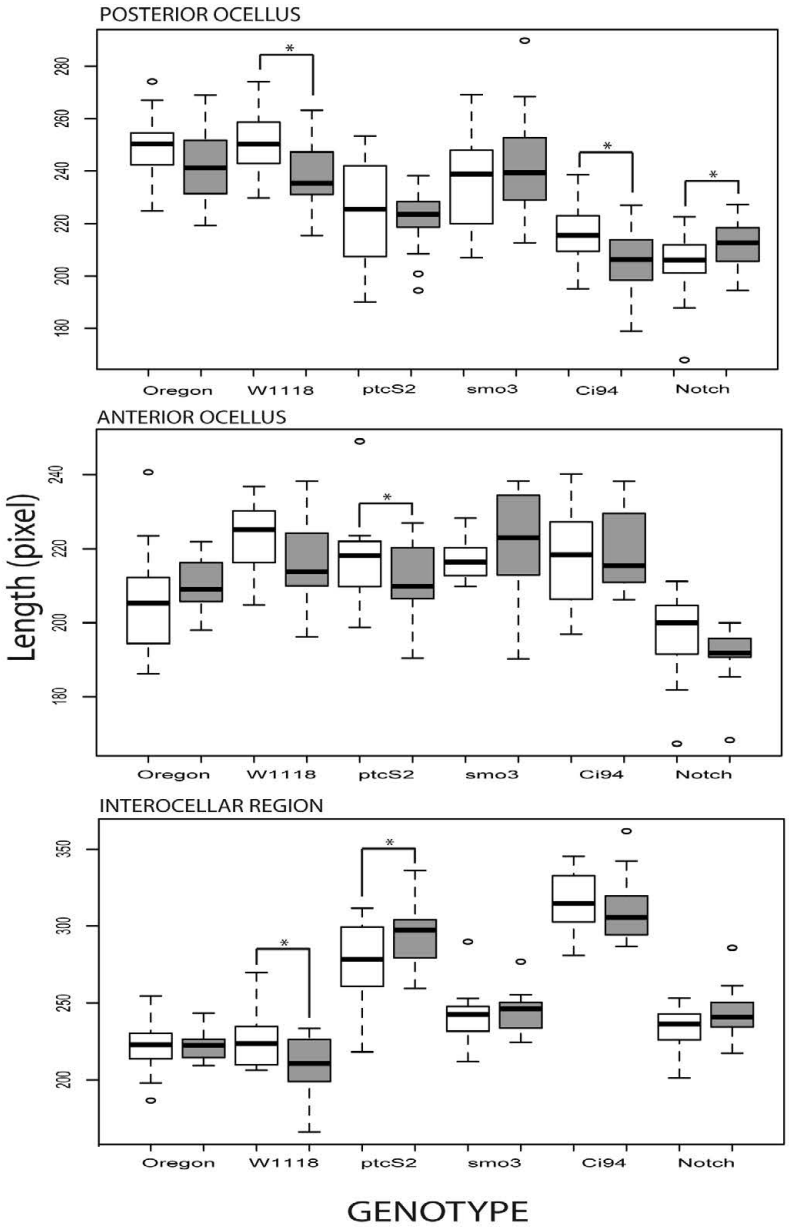

Coefficient of Variation (Cv) expressed in percentage

	Posterior Ocellus		Anterior Ocellus		Interocellar Region	
Oregon/Oregon*	4,72	5,98	3,94	4,39	7,29	4,71
W1118/W1118*	4,84	6,39	6,59	6,84	7,42	8,69
ptcS2/ptcS2*	8,23	5,04	4,98	3,09	11,15	6,48
smo3/smo3*	7,24	7,52	7,05	6,06	7,32	5,05
Ci94/Ci94*	5,23	5,99	4,93	7,27	5,95	6,57
Notch/Notch*	5,97	4,15	4,99	4,99	3,49	6,40

* with temperature cycles

Fig. S6. Quantitative variations in ocellar structures under temperature perturbations. Box plot showing measurements of the posterior ocellus, anterior ocellus and the interocellar region in the indicated genotypes. Length is expressed in pixels. White boxes represent strains grown at constant 25°C whereas gray boxes represent strains subjected to temperature cycles (see Materials and methods). Circles denote outliers above or below the inter-quartile range. Number of measured anterior ocelli, posterior ocelli and interocellar regions is 10, 20 and 20, respectively. Only females were included. Asterisks indicate significant differences between two experimental conditions (P<0.05). Below, the table contains the coefficient of variation within genotypes, expressed in percentage.

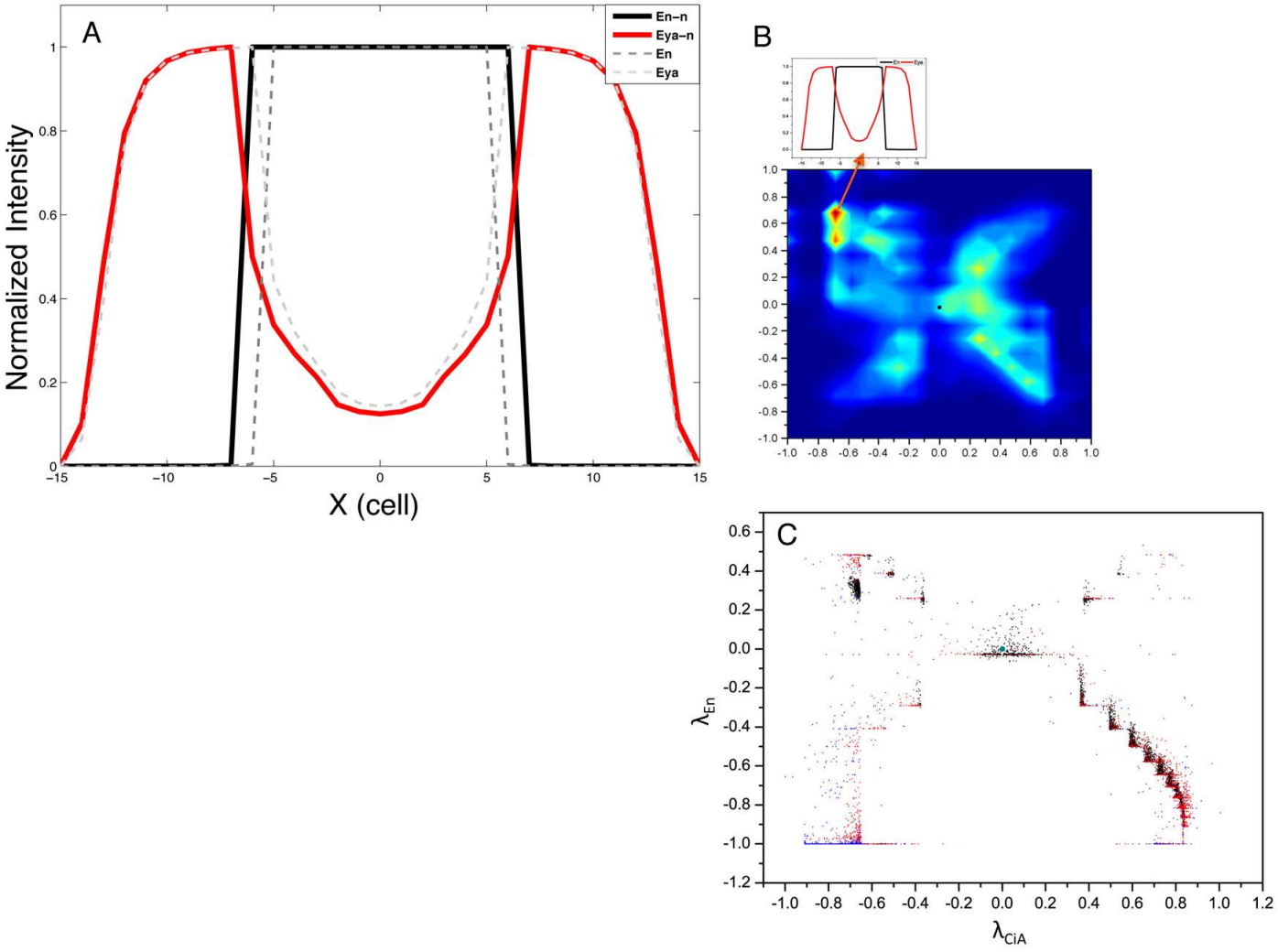

Fig. S7. Analysis of dense cluster pattern. (**A**,**B**) Noise effect on En and Eya profiles (A) over a specific pattern (B) situated in a dense cluster 'far', in global distance, from the wild type (0,0). (**C**) Projection of 10000 solution points corresponding to a randomized variation of all the sensitive parameters in ranges with complementary distance with value >0.8 (black dots), between 0.6 and 0.8 (red dots) and between 0.4 and 0.6 (blue dots). The projection is carried out on En and CiA distance patterns. There is significant overlap in the distribution of patterns generated by black, red and blue parameters, even though blue dots ('bad' parameters) tend to give patterns farther from (0,0).

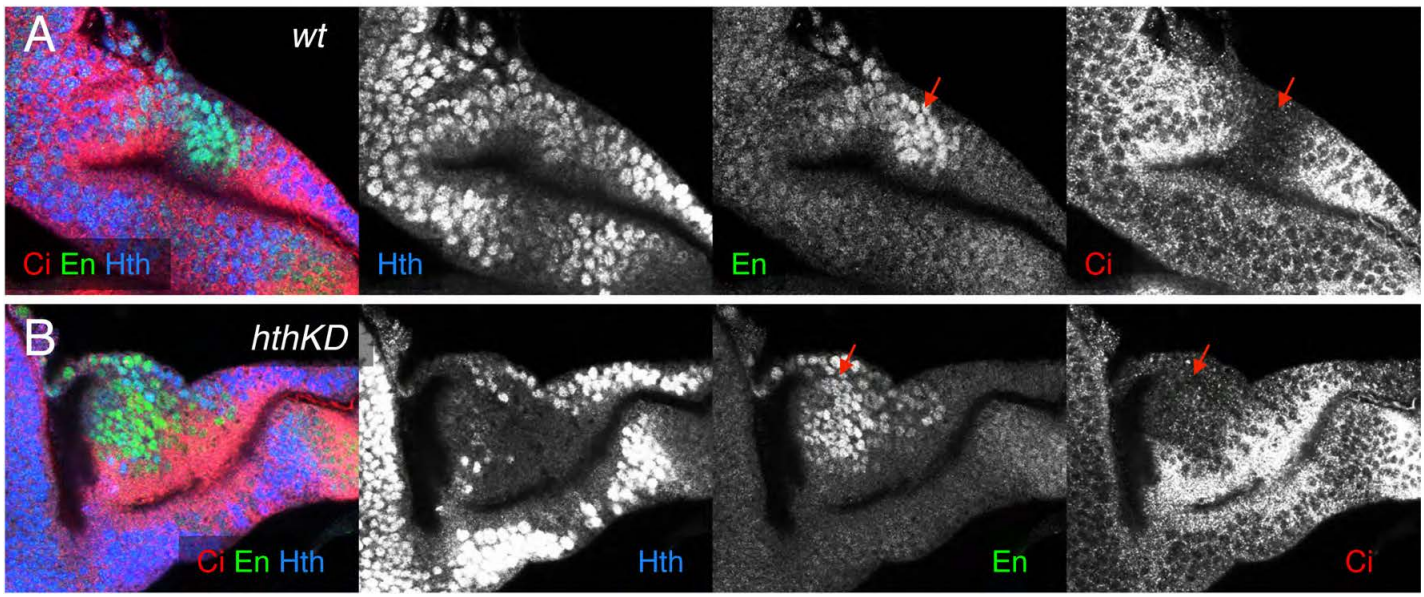

Fig. S8. *hth* regulates ocellar size without affecting *en* expression and its repression of the *hh* pathway. (**A**,**B**) Ocellar fields of control (A) and *oc2>hth(RNAi) (hthKD),* stained for Hth, En and Ci (B). In *hthKD* discs, Hth signal disappears in the whole ocellar field except for a few cells. In this genotype, *en* expression is detected at normal levels and Ci signal is downregulated in *en*-expressing cells. Red arrows indicate the En-expressing domain.

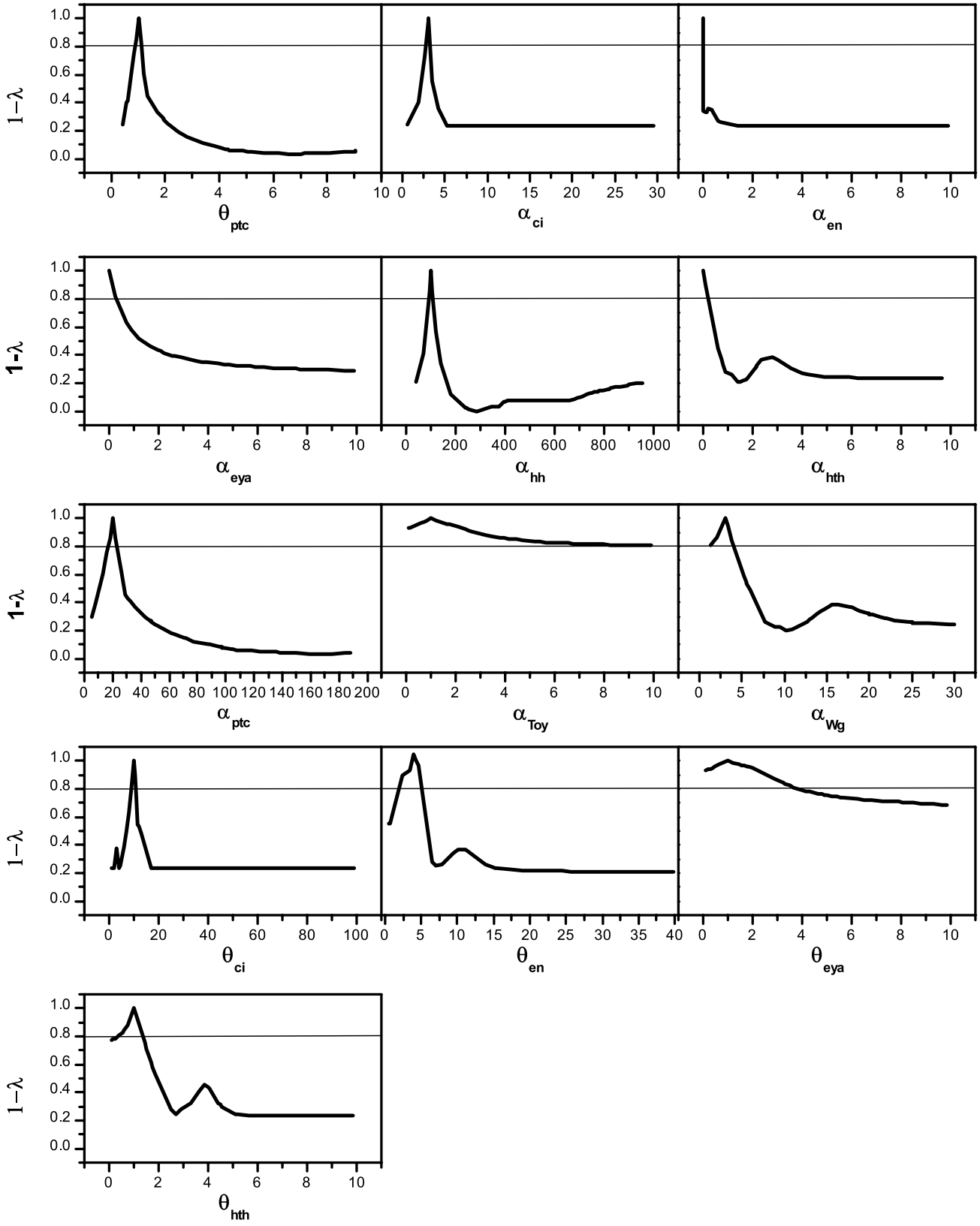

Fig. S9. Parameter sensitivity analysis plot. Goodness score (1–λ) for Eya pattern as a function of parameter values. λ is the Euclidean distance between the control Eya pattern and the pattern produced by a new value of the parameter. 1– λ was calculated for each parameter in a range of two orders of magnitude around the control value of the parameter. Goodness scores above 0.8 (line) are considered 'good' (i.e. within this range, the variation of the respective pattern results in Eya expression patterns closely resembling the control, or wild-type, pattern).

Table S1. Parameters and values used in the model. List of parameters used in the system with their control values. The list of parameters consists of different types: α_x for the basal transcription rates, β_x for the degradation rates, κ_x for the Hill equation transcriptional regulators, n_x for the Hill coefficients, θ_x for the translation rates; γ_{Ptc_Hh} for the protein complex formation of Ptc and Hh; the non-dimensional parameters κ_0, κ_{Ci}, κ_{En} and κ_{Ciptc} are different parameters used for changing the scale of different terms and D the diffusion coefficient. The values ranges correspond to a complementary distance to Eya wild-type pattern of (≥0.8), (≥0.6 and <0.8) and (≥0.4 and <0.6).

Parameter	Value	1-λ ≥ 0.8	0.6 ≥ 1-λ > 0.8	0.4 ≥ 1-λ > 0.6
α_{ci}	3	[2.75,3.27]	[2.24,2.75) ∪ (3.27,3.46]	[2.24,2.75) ∪ (3.27,3.46]
α_{en}	0	[0,0]	-	-
α_{eya}	0	[0,0.3]	(0.3,0.8]	(0.8,2.42]
α_{hh}	100	[91.2,106.6]	[80.2, 91.2) ∪ (106.6,117.6]	[67.03, 80.2) ∪ (117.6,132.96]
α_{hth}	0	[0,0.2]	(0.2,0.42]	(0.42,0.67]
α_{ptc}	20	[16.9,23.1]	[13.46, 16.9) ∪ (23.1,26.15]	[8.07, 13.46) ∪ (26.15,32.69]
α_{Toy}	1	[0.1,10]	-	-
α_{Wg}	3	[1.2,4.0]	(4.00, 5.06]	(5.06, 6.66]
β_{ci}	0.6	[0.1,6.0]	-	-
β_{CiA}	0.5	[0.37,0.64]	[0.20, 0.37) ∪ (0.64,0.81]	(0.81,1.00]
β_{CiR}	0.5	[0.4,0.65]	[0.26,0.4) ∪ (0.65,0.9]	(0.9,1.3]
β_{en}	0.1	[0.01,1.0]	-	-
β_{eya}	0.1	[0.01,1.0]	-	-
β_{Hh}	0.1	[0.03,0.22]	(0.22,0.34]	(0.34,0.72]
β_{hth}	0.1	[0.01,1.0]	-	-
β_{En}	0.5	[0.28,1.1]	[0.21,0.28) ∪ (1.1,1.55]	[0.14,0.21) ∪ (1.55,5]
β_{Eya}	0.1	[0.01,0.55]	-	-
β_{Hth}	0.5	[0.38,1.35]	-	-
β_{Ptc}	0.5	[0.38,0.67]	[0.3,0.38) ∪ (0.67,0.98]	[0.2,0.3) ∪ (0.98,1.63]
β_{ptc}	0.5	[0.05,5.0]	-	-
β_{PtcHh}	0.5	[0.43,0.57]	[0.36,0.43) ∪ (0.57,0.65]	[0.27,0.36) ∪ (0.65,1.04]
D	0.5	[0.4,0.57]	[0.24,0.4) ∪ (0.57,0.68]	[0.13,0.24) ∪ (0.68,2.6]
γ_{Ptc_Hh}	0.05	[0.045,0.11]	[0.04,0.045) ∪ (0.11,0.15]	[0.01,0.04) ∪ (0.15,0.25]
κ_0	10	[4.0,100]	-	-
κ_{Ci}	15	[12.1,19.6]	[9.3,12.1) ∪ (19.6,24.5]	[7.43,9.3) ∪ (24.5,51.9]
κ_{En}	2	[0.26,5.50]	[5.50,20]	-
κ_{Ciptc}	30	[19.87,40.0]	[10.89,19.87) ∪ (40,43.15]	[2,10.89) ∪ (43.15,74.3]
κ_{ci}	0.1	[0.01,0.216]	(0.216,0.40]	(0.4,0.78]
κ_{CiA}	2	[1.8,2.4]	[1.62,1.8) ∪ (2.40,2.72]	[1.11,1.62) ∪ (2.72,3.13) ∪ (3.81,8.99]
κ_{CiAen}	5	[3.46,9.95]	[2.80,3.46) ∪ (9.95,15.8]	[2.30,2.80) ∪ (15.8,50.0]
κ_{CiAeya}	7	[1.0,100]	-	-
κ_{CiAptc}	10	[6.26,21.2]	[3.72,6.26) ∪ (21.2,75.0]	[2.30,3.72) ∪ (75.0,100]
κ_{CiRen}	1	[0.76,1.24]	[0.49,0.76) ∪ (1.24,1.65]	[0.1,0.49) ∪ (1.65,2.27) ∪ (2.8,3.33]
κ_{CiRptc}	5	[1.7,18.4]	[0.8,1.7) ∪ (18.4,50]	-
κ_{DlEn}	0.2	[0.16,0.45]	[0.14,0.16) ∪ (0.45,0.91]	[0.01,0.14) ∪ (0.91,10]
κ_{Enci}	0.5	[0.1,1.1]	-	-
κ_{Enptc}	25	[5.1,250]	-	-
κ_{Eya}	20	[3.38,200]	-	-
κ_{Eyahth}	8	[0.8,80]	-	-
κ_{Htheya}	2	[1.58,5.0]	-	-
κ_{PH}	0.13	[0.11,0.14]	[0.1,0.11) ∪ (0.14,0.17]	[0.07,0.1) ∪ (0.17,0.24]

κ_{Wg}	2	[1.66,3.40]	-	-
n_{ci}	1	[1,2]	[3,100]	-
n_{CiA}	4	[4,5]	3 ∪ [6,10]	2 ∪ [11,100]
n_{CiAen}	1	[1,1]	[2,100]	-
n_{CiAeya}	9	[1,100]	-	-
n_{CiAptc}	1	[1,100]	-	-
n_{CiRen}	4	[4,4]	3,5	-
n_{CiRptc}	1	[1,5]	[6,100]	-
n_{En}	10	[7,100]	-	-
n_{Enci}	12	[4,100]	-	-
n_{Enptc}	5	[1,100]	-	-
n_{Eya}	2	[2,100]	-	-
n_{Hth}	2	[1,5]	-	-
n_{PH}	1	[1,1]	-	-
n_{Wg}	2	[2,3]	-	-
θ_{ci}	10	[9.12,10.6]	[7.58,9.12) ∪ (10.6,11.7]	[6.00,7.58) ∪ (11.7,14.3]
θ_{en}	4	[2.12,5.0]	[1.00,2.12) ∪ (5.00,5.50]	[0.62,1.00) ∪ (5.50,6.25]
θ_{eya}	1	[0.1,3.88]	[3.88,10.0]	-
θ_{hth}	1	[0.4,1.33]	[1.33,1.74]	[1.74,2.20) ∪ (3.60,4.10]
θ_{ptc}	1	[0.89,1.12]	[0.71,0.89) ∪ (1.12,1.19]	[0.55,0.71) ∪ (1.19,1.47]

Table S2. Initial condition for each system variable.

Variable	Description	Initial Condition
Hh	Hh concentration	0.1 μM
ptc	ptc concentration	0.1 μM
Ptc	Ptc concentration	0.1 μM
PtcHh	PtcHh complex concentration	0.1 μM
ci	ci concentration	0.1 μM
CiA	CiA concentration	0.1 μM
CiR	CiR concentration	0.1 μM
en	en concentration	0.01 μM
En	En concentration	0.01 μM
eya	eya concentration	0.1 μM
Eya	Eya concentration	0.1 μM
hth	hth concentration	0.75μM*
Hth	Hth concentration	1.5μM**

* Initial *hth* concentration correspond to its stationary value in the absence of Eya repression ($[hth]=\kappa_0\beta_{hth}\left(\alpha_{hth}+\alpha_{Wg}/k_{Wg}^{n_{Wg}}\right)$).** Initial Hth concentration corresponds to its stationary value ($[Hth]=\theta_{hth}[hth]/\beta_{hth}$). See table 1 for parameter values.

APPENDIX 1 FOR

A Hh-driven gene network controls specification, pattern and size of the *Drosophila* simple eyes.

D Aguilar-Hidalgo[§1,2], MA Domínguez-Cejudo[§1], G. Amore[3], A Brockmann[1,4], MC Lemos[2], A Córdoba[2], F Casares[1]*.

§- Equal contribution authors, listed in alphabetical order.

1- CABD (CSIC-UPO-Junta de Andalucía), Sevilla, Spain.
2- Condensed Matter Physics Dept. (U. Sevilla), Sevilla, Spain.
3- Stazione Zoologica Anton Dohrn, Napoli, Italy.
4- Current address: University of Konstanz, Germany

* Corresponding author: fcasfer@upo.es

Design and implementation of the ocellar mathematical model.

The design of this model is based on differential equations of the reaction-diffusion type. This model consists of 13 equations, one for each system variable (genes transcription and protein production) in a row of 31 cells with a symmetrical distribution of cells centered on the morphogen source (5 middle cells). Globally, the mathematical model comprises 403 ordinary differential equations (ODEs).

The design of the equation system follows the formulation paradigm used by von Dassow et al. (von Dassow et al., 2000). This methodology distinguishes between mRNA transcription and protein translation. Translation is described as linear terms of production and degradation. Transcriptional regulation is described with non-linear terms, either positive or negative, in the form of compound Hill equations. The specific form of these type of terms is $\phi(X\psi((Y,k_2,n_2),k_1,n_1)$, where

$$\phi(X,k,n)=\frac{X^n}{k^n+X^n} \qquad \text{(s1)}$$

and

$$\psi(Y,k,n)=\left(1-\frac{Y^n}{k^n+Y^n}\right), \qquad \text{(s2)}$$

so

$$\phi(X\psi(Y,k_2,n_2),k_1,n_1)=\frac{X^{n_1}\left(1-\frac{Y^{n_2}}{k_2^{n_2}+Y^{n_2}}\right)^{n_1}}{k_1^{n_1}+X^{n_1}\left(1-\frac{Y^{n_2}}{k_2^{n_2}+Y^{n_2}}\right)^{n_1}} \qquad \text{(s3)}$$

The ocellar model also contains autoregulations. In these cases, the equation term is described as a simple sigmoid in the form $\phi(X,k,n)$.

Parameter Sensitivity Analysis: one-by-one analysis.

Once a wild type set of parameter values had been found we tested whether these values are unique or if, on the contrary, it is possible to find different parameter sets that also lead to correct behaviors. One would expect that this latter option to be found, as organ development should be evolutionarily prepared to remain relatively constant in the face of fluctuations (i.e. to be robust) some of which may affect the biochemical properties of the gene networks controlling this development.

To analyze this issue, we carried out a parameter sensitivity analysis. The major problem we face is, once more, the large number of parameters. Therefore, we proceeded in two phases. In the first phase, we explored the parameter space modifying just one dimension (parameter) at a time; the rest of parameters are fixed to the "control" or wild type values. To do this, we defined a searching range for each parameter of two orders of magnitude around the "control" value for the wild type pattern. The resulting pattern was compared to the wild type and a goodness score obtained. This score represents the Euclidean distance (λ) between the Eya wild pattern and the Eya pattern drawn by the new set of parameters. To calculate the score, it was considered that both, the wild type (A) and the new (B) Eya patterns are described by two 31 component vectors (one component for each cell in the system). Then, the distance between these two vectors is defined as their Euclidean norm.

$$\lambda = \left|\left|\overrightarrow{AB}\right|\right| = \sqrt{\sum_i \left(b_i - a_i\right)^2} \qquad \text{(s4)}$$

where a_i and b_i are the components of vectors A and B, respectively.

In Sup. Figure S9 the distance distributions (considered as complementary distance, 1- λ) for all the system parameters are shown. From this analysis it is possible to extract important information about which parameters are more sensitive or more insensitive to variations away from the control parameter

values. In fact, some parameters can be considered quite insensitive, as their distances do not undergo significant changes.

A complementary distance value of 0.8 was selected as a "goodness" threshold, as every pattern checked for a parameter set with a complementary distance value equal or higher to this value fits the target ocellar pattern.

Following this "goodness" threshold, every parameter whose distance distribution falls below 0.8 is considered "sensitive" (33 parameters); and parameters whose distance distribution always remains above this threshold are considered "insensitive" (28 parameters). There are some parameters among the sensitive ones that are extremely sensitive as their variation range above the distance threshold is really small. The most restrictive parameter is α_{en}, which is responsible of the basal transcription of gene *en*. The wild type condition makes this parameter null. The sensitivity analysis predicts that this parameter should remain null or otherwise the distance value would fall.

At this point, we have determined which are the sensitive parameters and which can be freely varied without major consequence in the patterning. We have also established which are the ranges within which each sensitive parameter can be modified while the pattern obtained still remains within a given goodness distance interval.

Parameter Sensitivity Analysis: multiparametric analysis.

In the second phase we reconsidered the full parameter space exploration but eliminating from this study the insensitive parameters, and restricting the value ranges to those that give "good" patterning. Although these restrictions can be made, the resulting pattern is not assured to be "good", as the parameter space is still vast and the high complexity of the system might provide really "far" distance values just when modifying two parameters simultaneously. In order to be able to distinguish if the system can give "bad" patterns from "good" parameter values and, if "bad" parameter values always return "bad" profiles, a goodness scaling can be prepared. From the results in the parameter sensitivity analysis, we calculated, in addition to the "good" ranges, the parameter value ranges for distances between 0.6 and 0.8 ("medium"), and between 0.4 and 0.6 ("bad").

A total number of 10000 runs were obtained distributed in 6000 “good”, 3000 “medium” and 1000 “bad” randomized parameter values. With this 10000 parameter sets the distance for all the patterns of the system (one per variable) was calculated. In this way, each parameter set defines a point in a 13-dimensions space, each dimension being one of the model’s variables.

2D representation of the parameter sensitivity analysis

In order to represent the analysis, it was important to define a method to calculate a global distance in this hyperspace for visualizing the results in 2D. In the first place, the Euclidean norm does not distinguish sign, that is, it is not possible to know which of the patters, wild type and randomized, is bigger. So before calculating the norm it was determined which pattern defines a larger area under the curve. Thus, the distance between the two patterns is positive if the wild type pattern defines a larger area than the randomized pattern.

If we consider a 2D representation of the distance with sign, the wild type pattern would be placed in point (0,0). It is possible to plot just the distance from two different patterns out of 13 but this would just show the projection of the 13-dimentional points into 2D, and this projection may change depending on the two dimensions chosen for the plot. A method was implemented to visualize all the projections at one time.

To do so, first the normalized distance is divided into 0.1 length segments. Then the number of points in each 0.1x0.1 square for each projection of two variables was counted. The counting considered order, that is, the projection A-B is the same as B-A and just one of them is counted. This process is repeated for all the squares in the grid and for all the combinations of dimension pairs.

The result of this method can be seen in Figure 7F and Suppl. Fig. S7B. This plot represents the density of patterns from the 10000 randomized runs distributed relative to their distance from the wild type pattern. Therefore, this representation is a sort of phenotypic map produced by the network using the random sets of parameters.

Biological simplifications: The rationale for not including proliferation in the model, at least in this study, is the following: The development of the ocelli spans the second half of L3, that is, approximately 24 hours at 25^{o}C. Our estimate of the doubling rates in the eye field is about 13 hours (CS Lopes and FC, unpublished). Since the ocellar region does not express neither *eyg* nor *upd,* genes involved in stimulating cell proliferation in the eye field downstream of *Notch,* we expect the doubling rate in the ocellar field to be 13 hours or lower, therefore justifying our assumption.

Biological data used in the modeling of the Hh signaling pathway, including *en.*

The nuclear transducer of the Hh signaling pathway is encoded by *ci. ci* gives rise to an uncleaved form of Ci. In the absence of signal, Ci is processed proteolitically (and thus irreversibly) into a transcriptional repressor, CiR (Aza-Blanc et al., 1997; Methot and Basler, 1999). However, in the presence of signal, Ci is converted into a transcriptional activator, CiA. Hh signaling strength depends on the ratio between bound (to Hh) and unbound Ptc (Casali and Struhl, 2004), so that the higher this ratio, the more CiA (and the less CiR) is produced. CiA and CiR are thought to bind to similar DNA sequences in vivo to activate and repress, respectively, a similar set of targets genes. These include *en* and the Hh receptor *ptc* (Alexandre et al., 1996; Methot and Basler, 1999; Biehs et al., 2010). Therefore, in our model we assume a similar regulation for *ptc* and *en* in the ocellar region. In addition, *ci* basal transcription can be repressed by En (Schwartz et al., 1995). Another key element in the Hh pathway is the regulation of *ptc. ptc* transcription is positively regulated by Hh signaling and negatively by En. Then, the Ptc protein can bind to Hh. The Ptc:Hh complex is degraded after endocytosis, thereby making this association step irreversible.

Analysis of the Hh gradient steady state.

It is known that *hh* transcription is restricted to the interocellar region, known as *hh*-expressing zone. In this region $\delta(x) = 1$.

Once the morphogen gradient reaches its steady state ($t = t_{std}$) and Ptc is constant ([Ptc]), we have:

$$\left.\frac{\partial Hh}{\partial t}\right|_{t=t_{std}} = 0 \qquad \text{(s5)}$$

and,

$$D\frac{\partial^2 Hh}{\partial x^2} + \alpha_{hh} - \gamma_{Ptc\_Hh}[Ptc]\cdot Hh - \beta_{Hh}Hh = 0 \qquad \text{(s6)}$$

or,

$$D\frac{\partial^2 Hh}{\partial x^2} + \alpha_{hh} - \left(\gamma_{Ptc\_Hh}[Ptc] + \beta_{Hh}\right)Hh = 0 \qquad \text{(s7)}$$

The solution to this equation is:

$$Hh(x) = Hh_0 e^{-\frac{x}{\lambda}} - \frac{\alpha_{hh}}{\gamma_{Ptc\_Hh}[Ptc] + \beta_{Hh}} \qquad \text{(s8)}$$

The parameter $\lambda = \sqrt{D/\left(\gamma_{Ptc\_Hh}[Ptc] + \beta_{Hh}\right)}$ is known as decay length, which corresponds to the distance at which the morphogen concentration decays by a factor of *1/e*.

From Fick's first law we can assert that the morphogen production rate is given by:

$$\alpha_{hh} = -\frac{\partial Hh}{\partial x} \qquad \text{(s9)}$$

The flux direction is from higher concentration to lower concentration regions, being the flux a magnitude proportional to the gradient concentration. Thereby:

$$\alpha_{hh} = Hh_0\sqrt{D\left(\gamma_{Ptc\_Hh}[Ptc] + \beta_{Hh}\right)} \quad \text{at} \quad x = 0 \qquad \text{(s10)}$$

then,

$$Hh_0 = \frac{\alpha_{hh}}{\sqrt{D\left(\gamma_{Ptc\_Hh}\left[Ptc\right]+\beta_{Hh}\right)}} \tag{s11}$$

and,

$$Hh(x) = \frac{\alpha_{hh}}{\sqrt{D\left(\gamma_{Ptc\_Hh}\left[Ptc\right]+\beta_{Hh}\right)}} e^{-\frac{x}{\sqrt{D/\left(\gamma_{Ptc\_Hh}\left[Ptc\right]+\beta_{Hh}\right)}}} - \frac{\alpha_{hh}}{\gamma_{Ptc\_Hh}\left[Ptc\right]+\beta_{Hh}} \tag{s82}$$